Title

VISUAL network analysis reveals the role of BEH3 as a stabilizer in the secondary vascular development in Arabidopsis

Short title

BEH3 acts as a stabilizer in cambium.

Authors

Tomoyuki Furuya[1,2], Masato Saito[2], Haruka Uchimura[2], Akiko Satake[3], Shohei Nosaki[4], Takuya Miyakawa[4], Shunji Shimadzu[1,2], Wataru Yamori[2,4], Masaru Tanokura[4], Hiroo Fukuda[2], Yuki Kondo[1,2*].

Affiliations

[1] Department of Biology, Graduate School of Science, Kobe University, 1-1 Rokkodai, Kobe 657-8501, Japan.

[2] Department of Biological Sciences, Graduate School of Science, The University of Tokyo, Tokyo 113-0033, Japan.

[3] Department of Biology, Faculty of Science, Kyushu University, Fukuoka, 819-0395, Japan.

[4] Department of Applied Biological Chemistry, Graduate School of Agricultural and Life Sciences, The University of Tokyo, Tokyo 113-8657, Japan.

Corresponding author e-mail address

* Correspondence: pkondo@tiger.kobe-u.ac.jp

Abstract

During secondary growth in plants, vascular stem cells located in the cambium continuously undergo self-renewal and differentiation throughout the lifetime. Recent cell-sorting technique enables to uncover transcriptional regulatory framework for cambial cells. However, the mechanisms underlying the robust control of vascular stem cells have not been understood yet. By coexpression network analysis using multiple transcriptome datasets of an ectopic vascular cell transdifferentiation system using Arabidopsis cotyledons, VISUAL, we newly identified a cambium-specific gene module from an alternative approach. The cambium gene list included a transcription factor BES1/BZR1 homolog 3 (BEH3), whose homolog BES1 is known to control vascular stem cell maintenance negatively. Interestingly, the vascular size of the *beh3* mutants showed a large variation, implying the role of BEH3 as a stabilizer. BEH3 almost lost the transcriptional repressor activity and functioned antagonistically with other BES/BZR members via competitive binding to the same motif BRRE. Indeed, mathematical modeling suggests that the competitive relationship among BES/BZRs leads to the robust regulation of vascular stem cells.

42 **INTRODUCTION**

43

44 Continuous stem cell activity relies on a strict balance between cell proliferation
45 and cell differentiation. Plant vascular stem cells located in the cambium
46 proliferate by themselves, then continuously giving rise to conductive tissues
47 consisting of xylem and phloem cells, as bifacial stem cells (Shi et al., 2017; De
48 Rybel et al., 2016; Fischer et al., 2019). Previous genetic studies have indicated
49 that vascular stem cells are maintained by cell-cell communication via a peptide
50 hormone tracheary element differentiation inhibitory factor (TDIF) and its specific
51 receptor PHLOEM INTERCALATED WITH XYLEM (PXY) / TDIF RECEPTOR
52 (TDR) (Ito et al., 2006; Fisher et al., 2007; Hirakawa et al., 2008). For the
53 maintenance of vascular stem cells, the TDIF-PXY/TDR signaling promotes cell
54 proliferation via WUS-RELATED HOMEOBOX 4 (WOX4) and WOX14 (Hirakawa
55 et al., 2010, Etchells et al., 2010) and represses cell differentiation via BRI1-EMS-
56 SUPPRESSOR 1 (BES1) (Kondo et al., 2014). In addition, the TDIF-PXY/TDR
57 signaling genetically cross-talks with several peptide or hormonal signaling
58 pathways, thereby forming a complicated regulatory network (Han et al., 2018;
59 Etchells et al., 2012; Kondo and Fukuda, 2015). As another attempt to identify
60 stem cell regulators, transcriptome analysis using fluorescence activated cell
61 sorting (FACS) and fluorescence activated nuclear sorting (FANS) method has
62 been conducted. FACS transcriptome analysis with a (pro)cambium marker
63 *ARABIDOPSIS RESPONSE REGULATOR 15* (*ARR15*) *promoter:GFP* educed a
64 list of cambium-expressed transcription factors, including *AINTEGUMENTA*
65 (*ANT*), *KNOTTED-like from Arabidopsis thaliana 1* (*KNAT1*), *LOB DOMAIN-*
66 *CONTAINING PROTEIN 3* and *4* (*LBD3* and *LBD4*), *SHORT VEGETATIVE*
67 *PHASE* (*SVP*), and *PETAL LOSS* (*PTL*) (Zang et al. 2019). Furthermore, in the
68 inflorescence stem, FANS transcriptome analysis using tissue-specific promoters
69 including *PXY/TDR* promoter for proximal cambial cells and *SUPPRESSOR OF*
70 *MAX2 1-LIKE PROTEIN 5* (*SMXL5)* promoter for distal cambial cells provided
71 informative vascular tissue-specific gene expression profiles (Shi et al., 2020).

72 Nevertheless, the molecular mechanism enabling a robust control of vascular
73 stem cells remains largely unknown.
74 The vascular system consists of various types of vascular cells at
75 different developmental stages, preventing the sequential analysis of vascular
76 development with a focus on bifacial stem cells. To simply understand a complex
77 biological phenomenon such as vascular development, reconstitutive approach
78 has great experimental advantages with regard to molecular genetic studies
79 (Kondo 2018). We previously established a tissue culture system, Vascular cell
80 Induction culture System Using Arabidopsis Leaves (VISUAL), which can
81 synchronously and efficiently induce xylem and phloem cells from mesophyll cells
82 via vascular stem cell (Kondo et al., 2016). The loss-of-function mutant for the
83 phloem regulator ALTERED PHLOEM DEVELOPMENT (APL) lacks phloem
84 sieve element differentiation. In addition to the microarray data with the *apl*
85 mutants, the datasets of the FACS with a phloem marker gene, *SIEVE ELEMENT*
86 *OCCLUSION RELATED 1* (*SEOR1*) in VISUAL enabled the construction of a
87 coexpression gene network from early to late phloem sieve element
88 differentiation process (Kondo et al. 2016). Although such a network analysis is
89 useful for temporal dissection of vascular differentiation process, this gene
90 network is still only limited to phloem sieve element differentiation. Recently, we
91 discovered that the loss-of-function *bes1* mutants showed a dramatic impairment
92 in the differentiation of xylem and phloem cells, resulting in the accumulation of
93 vascular stem cells in the VISUAL (Kondo et al., 2014; Saito et al., 2018; Kondo
94 et al., 2015). Then we further integrated *bes1* transcriptome and time-course
95 (every 6 hours) transcriptome datasets in order to visualize the gene network for
96 the entire vascular differentiation process.
97 In this study, we newly established a coexpression network of the
98 VISUAL differentiation process utilizing multiple transcriptome datasets including
99 the *bes1* mutants. As a result, we succeeded in the identification of gene modules
100 corresponding to not only phloem but also xylem and cambial cells. These
101 classifications were validated with a comparison to the already-existing vascular
102 FACS and FANS datasets. Through the network analysis, one of BES/BZR

homolog BEH3 was found as a potential vascular stem cell regulator. Indeed, a knock-out mutant of BEH3, *beh3-1*, exhibited a high variation in vascular size among individual samples, suggesting that BEH3 functions as a stabilizer of vascular stem cells. Further genetic and molecular studies revealed that BEH3 has an opposite function toward other BES/BZR homologs by interfering with other BES/BZR homologs via competitive binding to the BR response element (BRRE). Moreover, mathematical modeling analysis showed that the competitive relationship among BEH3 and other BES/BZR homologs enables the robust control of vascular stem cells.

RESULTS

Coexpression network analysis using the multiple VISUAL transcriptome datasets identifies a cambium-related gene module

To find out novel regulators for vascular stem cells, we conducted a gene network analysis using the transdifferentiation system VISUAL (Figure 1A; Kondo et al., 2015). First, we selected 855 VISUAL-induced genes that were up-regulated highly (more than eight-fold) in microarray data (0 h vs 72 h after VISUAL induction) (Figure 1B; Supplemental Data set 1). Since the selected 855 VISUAL-induced genes should include xylem-, phloem- and cambial-related genes, we constructed a coexpression gene network for these genes with the use of multiple VISUAL transcriptome datasets including (1) 6-h interval time-course, (2) cell-sorting with the phloem marker *pSEOR1:SEOR1-YFP*, (3) phloem deficient *apl* mutants, and (4) *bes1-1* mutants (Figure 1A). Here the *bes1-1* mutant transcriptome datasets were used for dissecting cambial cells and differentiated xylem/phloem cells, because the *bes1-1* mutants significantly accumulate cambial cells due to the inhibition of xylem and phloem differentiation in the VISUAL (Figure 1A). Coexpression network using the WGCNA package divided the 855 VISUAL-induced genes into four distinct modules (Module-I to IV) and 11 outgroup genes (Others, O) (Figure 1C). Expression of Module-III and -IV genes were down-regulated in the *bes1-1* mutants (Figure 1C), suggesting that these

134 modules were considered as differentiated xylem and phloem cells-related ones.
135 In addition, expression of Module-III genes was high in the SEOR1-positive cell-
136 sorting datasets and was down-regulated in the *apl* mutants, whereas expression
137 of Module-IV genes was unchanged in the cell-sorting and the *apl* mutant
138 datasets (Figure 1D), suggesting that Module-III and -IV represents phloem-
139 related and xylem-related genes, respectively. Consistent with this idea, the
140 known phloem-related genes such as *RAB GTPASE HOMOLOG C2A* (*RABC2A*),
141 *BREVIS RADIX* (*BRX*), *GLUCAN SYNTHASE-LIKE 7* (*GSL07*), and *NAC*
142 *DOMAIN CONTAINING PROTEIN 45* (*NAC045*), were found in Module-III,
143 whereas xylem-related genes such as *IRREGULAR XYLEM 3* (*IRX3*), *XYLEM*
144 *CYSTEINE PEPTIDASE 1* (*XCP1*), and *VASCULAR-RELATED NAC-DOMAIN 6*
145 (*VND6*), were in Module-IV (Figure 1C). On the other hand, expression of
146 Module-I and -II genes was induced at earlier timing and was remained higher
147 even in the *bes1-1* mutants than that of Module-III and -IV genes (Figure 1B and
148 1D), suggesting that Module-I and -II genes correspond to (pro)cambial-related
149 genes. To validate these characterizations, we investigated gene expression of
150 each module in the transcriptome datasets of FACS in roots and FANS in stems
151 obtained using the cell-type specific markers (Brady et al. 2007, Zang et al. 2019,
152 Shi et al. 2020). Expectedly, expression of Module-III and -IV genes were quite
153 high in the phloem specific *APLpro* datasets and the xylem specific *S18* and
154 *VND7pro* datasets, respectively (Figure 1E; Supplemental Figure 1A). As for
155 Module-I and II, the genes in Module-I were relatively highly expressed in the
156 procambium (ARRIII ± BAP) and expression of Module-II gene is more specific
157 to the developing cambium and cambium (ARRI ± BAP and ARRII ± BAP) in the
158 FACS datasets (Figure 1E). These results suggest that Module-I and Module-II
159 represents procambium-related and cambium-related genes, respectively.
160 Consistent with this idea, expression of Module-I genes was expressed much
161 earlier than that of Module-II genes (Figure 1B).
162 We further analyzed the Module-II genes for analyzing stem cell
163 regulation. The Module-II consists of a total of 394 genes including some known
164 cambium-related genes, such as *PYX/TDR*, *SMXL5*, *ANT*, *LBD3*, *LBD4*, and

165 *HOMEOBOX GENE 8* (*HB-8*) (Figure 1B – 1D). Of them, 32 genes encoding
166 transcription factors were investigated in more detail (Supplemental Data set 2).
167 Previous studies have revealed that vascular stem cells locate in the overlapped
168 region of *PXY/TDR* and *SMXL5* expression, which marks proximal/xylem and
169 distal/phloem side of cambium, respectively (Shi et al. 2019). According to the
170 FANS transcriptome datasets (Shi et al., 2020), 13 out of the 32 transcription
171 factor genes are expressed mainly in *PXY/TDRpro* and/or *SMXL5pro* (Figure 1F).
172 They included not only known cambial regulators such as *ANT* (Randall et al.,
173 2015) and *LBD4* (Zang et al., 2019; Smit et al., 2020), but also novel candidates
174 such as *BEH3*, *DOF AFFECTING GERMINATION 1* (*DAG1*), and *At1g63100*
175 (Figure 1E). The analysis of these newly selected genes may provide a novel
176 insight into regulation of cambial activity.
177
178 **BEH3 stabilizes secondary vascular development**
179 We recently showed that BES1 and its closest homolog BRASSINAZOLE
180 RESISTANT1 (BZR1) redundantly function to promote vascular stem cell
181 differentiation in VISUAL (Saito et al., 2018). Therefore, we chose BEH3 as a
182 potential vascular stem cell-specific regulator for further studies. Among 6
183 BES/BZR homologs in *Arabidopsis thaliana*, only *BEH3* was found in the
184 cambium-related module. Indeed, only *BEH3* expression levels were remarkably
185 increased in the time course RNA-seq data of the VISUAL (Figure 2B), and the
186 GUS expression domain of *pBEH3:GUS* gradually expanded over time (Figure
187 2C). Consistent with the observation in the VISUAL, *pBEH3:GUS* was
188 preferentially expressed in the vascular tissues including cambium of leaves and
189 hypocotyls (Figure 2D and 2E). Then to investigate the function of BEH3 in
190 vascular development, we analyzed the BEH3 knock-out mutant, *beh3-1*, which
191 has a T-DNA insertion on its 1st exon (Lachowiec et al., 2018). Here we
192 compared vascular secondary growth in the WT and the *beh3-1* mutants grown
193 under short-day condition. The area inside the cambium in the *beh3-1* mutants
194 were slightly but significantly decreased when compared with the WT (Figure 2F
195 and 2G; Supplemental Figure 2). In addition, we realized that the *beh3-1* mutants

196 seem to have a higher variation in area inside the cambium than the WT (Figure
197 2H). Indeed, the values of coefficient of variation (CV) between the *beh3-1*
198 mutants and WT plants were significantly different in two statistical analyses:
199 asymptotic and Modified signed-likelihood ratio test (M-SLRT) (Feltz and Miller,
200 1996; Krishnamoorthy and Lee, 2014) (Figure 2I). These results suggest that the
201 presence of BEH3 contributes to not only promoting but also stabilizing
202 secondary vascular development.
203
204 **BEH3 functions oppositely to BES1 in vascular development**
205 In *Arabidopsis thaliana*, 6 BES/BZR transcription factors have the redundant
206 function in brassinosteroid (BR) signaling (Yin et al., 2005; Lachowiec et al.,
207 2018; Chen et al., 2019a; Chen et al., 2019b; Nolan et al., 2020). As previously
208 reported (Kondo et al., 2014; Saito et al., 2018), *bes1-D*, which has a mutation in
209 protein degradation PEST sequence, exhibited a reduced number of (pro)cambial
210 cell layers between differentiated xylem (red) and phloem (green) in hypocotyls
211 (Figure 3A). To compare the function of BEH3 and BES1, vascular phenotype of
212 gain-of-function mutant for BEH3 was analyzed. Since BEH3 does not possess
213 any obvious PEST domain, we generated a transgenic stable line of β-estradiol-
214 inducible BEH3 overexpressor (*pER8:BEH3-CFP*). In contrast to the *BES1* gain-
215 of-function mutants, *BEH3* overexpression lines showed an increase in the
216 number of (pro)cambium layers (Figure 3B). In association with this tendency,
217 the vascular area was also enlarged in the two independent *BEH3*
218 overexpression lines (Figure 3C and 3D; Supplemental Figure 3), which is not
219 contradictory to the *beh3-1* mutant phenotype. These results suggest that BEH3
220 has an opposite function to BES1 during secondary vascular development.
221 As described above, the *bes1-1* mutants disrupt cell differentiation from
222 vascular stem cells in the VISUAL (Figure 1A). To investigate the function of
223 BEH3 and other BES/BZR homologs, we evaluated the contribution of each
224 BES/BZR homolog to xylem differentiation with a semi-automatic calculation
225 method using a xylem indicator, BF-170 (Nurani et al., 2020) in VISUAL (Figure
226 4A and 4B; Supplemental Figure 4). As for the analysis with single mutants, *beh4-*

227 *1* as well as *bes1-1* and *bzr1-1* showed reduced xylem differentiation ratio in the
228 VISUAL compared with the WT (Fig. 4C and 4D; Supplemental Figure 5),
229 indicating that BEH4 also promotes xylem differentiation. On the other hand,
230 xylem differentiation ratio in *beh3* as well as *beh1* and *beh2* were comparative to
231 the WT (Figure 4B and 4C). Next, we examined the impact of mutating a BES1
232 homolog in the *bes1-1* mutant background as double mutants. Only the *bes1-1*
233 *beh3-1* double mutants showed a high xylem differentiation ratio, similar to that
234 observed in the WT, whereas none of the other mutants rescued the *bes1*
235 phenotype (Figure 4B and 4C; Supplemental Figure 5 and 6). The *bes1* mutants
236 disrupt the differentiation from vascular stem cells into not only xylem but also
237 phloem cells (Saito et al., 2018), accompanied by the decrease in expression
238 levels of xylem-specific (*IRX3*) and phloem-specific (*SEOR1*) marker genes
239 (Figure 4E). This reduction in the *bes1-1* mutants was recovered up to WT levels
240 by the additional *beh3-1* mutation (Figure 4E). Quantitative expression analysis
241 also indicated that the single *beh3-1* mutants slightly increase the expression
242 levels of *IRX3* and *SEOR1* at 48 h, when compared to the WT (Figure 4E;
243 Supplemental Table 1). These genetic data suggest that BEH3 functions
244 oppositely to BES1 also in the VISUAL.
245
246 **BEH3 has a competitive relationship with other BES/BZR homologs**
247 To unravel the molecular basis of the antagonistic function of BEH3, we
248 examined the functional difference among BEH3 and other BES/BZR proteins.
249 Amino acid sequence alignments suggested no obvious difference in the known
250 functional domains/motifs, such as DNA-binding domain (DBD) and EAR motif
251 (Yin et al., 2002; Wang et al., 2002; Oh et al., 2014). It is known that BES1 and
252 BZR1 repress the transcription of a BR biosynthetic gene, *DWARF4* (*DWF4*), by
253 directly binding to the BRRE and/or E-box motif in the *DWF4* promoter (He et al.,
254 2005; Sun et al., 2010; Yu et al., 2011; Chung et al., 2011; Nosaki et al., 2018).
255 Therefore, we tested the transcriptional control activity of BES/BZR members
256 against the *pDWF4: Emerald Luciferase (ELUC)* construct transiently expressed
257 in *Nicotiana benthamiana* leaves. The signal intensity of ELUC gradually

258 decreased from 3 to 9 h after activating BES1, BZR1, and BEH4 by induction
259 system using dexamethasone (DEX) and rat glucocorticoid receptor (GR)
260 (Aoyama et al., 1995), whereas BEH3 activation did not alter ELUC activity
261 (Figure 5A). Electrophoretic mobility shift assay (EMSA) for the BRRE core motif
262 and E-box motif with DBD of BES/BZR members indicated that BEH3 can bind
263 to the BRRE and E-box, similar to BES1, BZR1, and BEH4 (Nosaki et al., 2018)
264 (Figure 5B; Supplemental Figure 7). These results suggest that BEH3 binds to
265 the BRRE and E-box motif but exhibits much lower transcriptional repressor
266 activity than other BES/BZR homologs. When BEH3 and BES1 were
267 simultaneously expressed in *N. benthamiana* leaves, repressor activity of BES1
268 against *pDWF4:ELUC* was weakened (Supplemental Figure 8). By contrast, co-
269 expression of BZR1 with BES1 did not show such a combinatory repressive effect
270 (Supplemental Figure 8), suggesting the possibility that BEH3 interferes with
271 other BES/BZR homologs via the binding competition.
272 In the VISUAL, the mutation in *BES1* did not affect *BEH3* expression, and
273 the mutation in *BEH3* did not affect *BES1* expression in VISUAL (Supplemental
274 Figure 9), indicating that there seems not to be an epistatic relationship between
275 *BEH3* and *BES1*. Then to genetically investigate the competitive relationship
276 among *BEH3* and other *BES/BZR* homologs, several combinations of triple
277 mutants were analyzed in VISUAL. Although the *beh3-1* mutant allele could
278 completely rescue the phenotype of the *bes1-1* single mutants (Figure 4B – 4D),
279 restoration of xylem differentiation by the *beh3-1* mutant allele was only partial in
280 the background of *bes1-1 bzr1-2* double mutants (Figure 4F and 4G). Such a
281 partial rescue was not detected in the *bes1-1 bzr1-2 beh4-1* triple mutants at all
282 (Figure 4F and G). Consistent with the xylem differentiation ratio, the *bes1-1 bzr1-*
283 *2 beh3-1* triple mutants were intermediate between WT and the *bes1-1 bzr1-2*
284 double mutants in terms of expression levels of xylem and phloem marker genes
285 (Figure 4H). Taken together, these results suggest that BEH3 acts
286 antagonistically with other homologs in a competitive manner in the VISUAL.
287

288 **Competitive inhibition by BEH3 may be limited to the transcriptional**
289 **repressor activity of other BES/BZR homologs**
290 Previous studies showed that a *bes1* hextuple mutants, in which all BES/BZR
291 members are knocked-out, exhibits male sterility (Chen et al., 2019a). If BEH3
292 always has a competitive role against other BES/BZR homologs, *bes1 bzr1 beh1*
293 *beh2 beh4* quintuple mutants are expected to show the same phenotype as *bes1*
294 *bzr1 beh1 beh2 beh3 beh4* hextuple mutants. Then we generated a *bes1*
295 hextuple mutants (*bes1-1 bzr1-2 beh1-2 beh2-5 beh3-3 beh4-1*) and a *bes1*
296 quintuple mutants (*bes1-1 bzr1-2 beh1-2 beh2-5 beh4-1*) using CRISPR/Cas9
297 system. Consistent with the previous reports, the newly established *bes1*
298 hextuple mutants showed shorter siliques with no seed (Figure 6A and 6B;
299 Supplemental Figure 10). However, the *bes1* quintuple mutants successfully
300 produced seeds in siliques (Figure 6A and 6B). In addition, while the primary root
301 length of the *bes1* hextuple mutants were shorter than the WT, that of the *bes1*
302 quintuple mutants were comparable to the WT (Figure 6C and 6D). These results
303 suggest that BEH3 partially remains the same function to other BES/BZR
304 homologs.
305 BES1 and BZR1 is known to function as both transcriptional activators
306 and repressors (Yin et al., 2005; He et al., 2005; Nolan et al., 2020). Then, we
307 investigated to which extent BEH3 affects the expression of known BES/BZR-
308 target genes in planta. Here we used the β-estradiol-inducible *BEH3*
309 overexpressor *pER8:BEH3-CFP,* in which expression of *BEH3* was increased
310 upon β-estradiol treatment (Figure 6E; Supplemental Figure 11). *DWF4* and
311 *BRASSINOSTEROID-6-OXIDASE 2* (*BR6ox2*), as BES1-direct repressed genes
312 (He et al., 2005; Sun et al., 2010; Yu et al., 2011), were remarkably repressed in
313 the constitutively active mutant for *BES1* and *BZR1* (*bes1-D bzr1-D*) (Figure 6F),
314 whereas *pER8:BEH3-CFP* transgenic plants significantly increased the mRNA
315 levels of both *DWF4* and *BR6ox2* upon β-estradiol treatment (Figure 6E;
316 Supplemental Figure 11; Supplemental Table 2). These results suggest that the
317 non-canonical BEH3 can passively inhibit the transcriptional repressor activity of
318 endogenous BES1 homologs by competing for the same binding motif. However,

319 *BEH3* overexpression did not suppress mRNA levels of BES1-direct activated
320 genes, *SAUR-AC1* and *INDOLE-3-ACETIC ACID INDUCIBLE 19* (*IAA19*) (Yin et
321 al., 2005; Sun et al., 2010; Oh et al., 2012) (Figure 6E), whose expression was
322 highly induced in the *bes1-D bzr1-D* double mutants (Figure 6F). Together with
323 the genetic results of the *bes1* high-order mutants, our results suggest that
324 competitive relationship among BES/BZR members may be limited mainly to their
325 transcriptional repressor activity.
326
327 **BEH3 contributes to increasing robustness via the competition with other**
328 **homologs**
329 Our observation revealed that the *beh3* mutants increased the variation in the
330 size of vascular area (Figure 2). Then to understand the significance of the
331 competitive relationship between BEH3 and other BES/BZR members in
332 phenotypic variation, a mathematical model for competitive binding was
333 constructed with a focus on the transcriptional repressor activity. In this
334 mathematical modeling, we set the repressor activity of BEH3 and other
335 homologs at 0.95× and 0.8×, respectively, when they occupied one binding site
336 in the target gene promoter. Here, we assumed three binding sites in the putative
337 promoter and predicted the output as vascular cell number, when the binding rate
338 of BEH3 (P_{BEH3}) and other homologs (P_O) was varied (Figure 7A). When P_{BEH3}
339 was increased, the average predicted outputs went up because the accessibility
340 of the binding sites for other homologs was decreased (Figure 7B). This
341 competitive modeling can account for the phenotype that *BEH3* overexpression
342 leads to the enlargement of vascular area (Figure 3C and 3D). On the other hand,
343 further modeling revealed that a reduction in P_{BEH3} decreased the means of
344 output value, which corresponds to smaller area inside the cambium in the *beh3-*
345 *1* mutants when compared with the WT (Figure 2F - 2H). Moreover, because the
346 *beh3-1* mutants exhibited higher variation in the vascular size than the WT
347 (Figure 2F - 2H), we also simulated the shift of the CV when the value of P_{BEH3}
348 was decreased. As a result, a reduction in P_{BEH3} increased the CV of the output
349 (Figure 7C), which mimics the vascular phenotype of the *beh3-1* mutants.

350 Collectively, our results indicate that the cambium-expressed BEH3 competitively
351 inhibits transcriptional repressor activity of other BES/BZR homologs, thereby
352 minimizing the fluctuation of the vascular stem cell activity.
353
354 **DISCUSSION**
355 In this study, we constructed the gene coexpression network during the VISUAL
356 differentiation process (Figure 1). With the help of the existing FACS and FANS
357 transcriptome datasets, our network analysis categorized vascular-related genes
358 into four distinct modules; procambium (Module-I), cambium (Module-II), phloem
359 (Module-III) and xylem (Module-IV). Thus, reconstitute approach using the
360 VISUAL is effective to dissect a hierarchical process of vascular cell
361 differentiation and helpful for isolating genes involved in this process. Although
362 the FACS datasets (Zang et al. 2019) almost share a similar tendency with our
363 network prediction (Figure 1; Supplemental Figure 1), the overlapping rate of
364 cambial genes was not so high (12.9 %, 45 genes/394 genes of Module- II). The
365 low rate may result from differential cell state of cambium/vascular stem cells
366 between "*in vivo*" and "*in vitro*" and/or technical differences between cell-sorting
367 and whole tissue sampling. Therefore, combinatory approach by bioinformatics
368 will allow the accurate and efficient identification of gene-of-interest expressed in
369 the vasculature, which is usually masked by its deep location. Indeed, we
370 successfully identified a novel cambium regulator BEH3 in the gene lists
371 combined the Module-II genes with the FANS datasets (Shi et al., 2020). Also in
372 the xylem and phloem development, there remain so many unidentified genes.
373 Moreover, it is poorly understood how the cambium is established after
374 procambium development. Therefore, our coexpression network will be
375 informative for further studies on the sequential vascular development.
376 Although previous studies indicated redundant roles of BES/BZR family
377 members in BR signaling (Yin et al., 2005; Lachowiec et al., 2018; Chen et al.,
378 2019a; Chen et al., 2019b; Nolan et al., 2020), little has been reported about their
379 functional differences. Here we found BEH3 as a non-canonical member of the
380 BES/BZR family. *BEH3* is expressed preferentially in the vascular cambium,

381 whereas *BES1* and *BZR1* expression is observed ubiquitously (Yin et al., 2002).
382 Moreover, our results indicated the opposite function between BEH3 and BES1.
383 In the context of *in vivo* vascular development, the gain-of-function *bes1-D*
384 mutants accelerate cell differentiation of vascular stem cells and consequently
385 decreased the number of (pro)cambial cell layer, eventually resulting in
386 diminishment of the vascular size (Figure 2) (Kondo et al., 2014). Conversely,
387 *BEH3* overexpression led to the increase in the number of (pro)cambial cell layer
388 with enlargement of the vascular size. Consistently, the *beh3* loss-of-function
389 mutants showed a decreased size of vascular area. Considering that BEH3 has
390 a repressive effect on vascular cell differentiation in the VISUAL, these results
391 suggest that BEH3 has a positive role in the maintenance of vascular stem cells
392 probably by inhibiting excess cell differentiation (Figure 7D). Molecular analyses
393 suggested that BEH3 retains a binding capability to the BRRE but loses a
394 transcriptional repressor activity. Such a competitive action leads to the opposite
395 behavior of BEH3. As a similar example in mammals, JunB, a transcription factor,
396 exhibits weaker activity than its homolog, c-Jun, can repress c-Jun-mediated
397 transactivation (Deng and Karin, 1993). In this study, our modeling and genetic
398 analysis with the *beh3* mutants suggested that the presence of a weak or non-
399 active type member in a transcription factor family enables a fine-tuned control of
400 signaling outputs.
401 Taken together, we conclude that the competition among BES/BZR
402 family members in the cambium potentially enables the stable and robust
403 maintenance of vascular stem cells for ensuring continuous radial growth.
404 However, it remains unclear why only BEH3 partially lacks the transcriptional
405 repressor activity and why the competitive suppression by BEH3 is limited to the
406 repressor activity. Further comparative interactome analysis between BEH3 and
407 other BES1 homologs will uncover the mechanism underlying functional
408 differences among BES/BZR proteins.
409
410 **METHODS**
411

412 **Plant materials**

413 Seeds of *Arabidopsis bes1-1* (SALK_098634), *beh1-1* (SAIL_40_D04), *beh3-1*
414 (SALK_017577), and *beh4-1* (SAIL_750_F08) mutants were obtained from the
415 Arabidopsis Biological Resource Center (ABRC), Ohio, USA. The *bzr1-1* single
416 mutants and *bes1-1 bzr1-2* double mutants were generated previously using the
417 CRISPR system (Saito et al., 2018), and *bes1-1 beh1-1*, *bes1-1 beh3-1*, *bes1-1*
418 *beh4-1*, *bes1-1 bzr1-2 beh3-1,* and *bes1-1 bzr1-2 beh4-1* mutants were
419 generated by crossing. Chen et al. reported that the *bes1-1* mutants expresses
420 one of the two splice variants of *BES1* (*BES1-S*); however, the other splice variant
421 (*BES1-L*), which is functionally more important, is completely eliminated (Chen at
422 al., 2019b, Jiang et al., 2015). The *bes1-1 bzr1-2 beh2-5 beh4-1* quadruple
423 mutants were generated by the CRISPR/Cas9 system using pKAMA-ITACH
424 vector (Tsutsui et al., 2017). The single guide RNA (sgRNA; Supplemental table
425 3.) sequence corresponding to the target gene, *BEH2*, was cloned into the
426 *pKIR1.1* vector. The resulting construct was transformed into the *bes1-1 bzr1-2*
427 *beh4-1* triple mutants. In the T2 generation, *Cas9*-free plants with homozygous
428 *beh2-5* mutation were selected as described previously (Tsutsui et al., 2017). The
429 *bes1* quintuple mutants (*bes1-1 bzr1-2 beh1-2 beh2-5 beh4-1*) were also
430 generated using the CRISPR/Cas9 system, which targeted the *BEH1* locus in
431 *bes1-1 bzr1-2 beh2-5 beh4-1*. To generate the *bes1-1 beh3-2* double mutants
432 and *bes1* hextuple mutants (*bes1-1 bzr1-2 beh1-2 beh2-5 beh3-3 beh4-1*), the
433 *BEH3* locus was edited using the CRISPR/Cas9 system in *bes1-1* single mutants
434 and *bes1* quintuple mutants, respectively. To generate a construct for *BEH3*
435 overexpression under the control of a β-estradiol-inducible promoter, the coding
436 sequence of *BEH3* (At4g18890.1) was amplified from Col-0 cDNA by PCR and
437 then cloned into pENTR/D-TOPO (Life Technologies). Using LR clonase II (Life
438 Technologies), the region between *attL1* and *attL2* in the entry vector was cloned
439 into the destination vector, pER8-GW-CFP, which expressed the cyan
440 fluorescent protein (CFP)-tagged proteins upon estrogen application (Ohashi-ito
441 et al., 2010). To generate the *pBEH3:GUS* construct, a 1,997 bp fragment
442 upstream of *BEH3* was amplified from Col-0 genomic DNA by PCR and cloned

443 into pENTR/D-TOPO. The region between *attL1* and *attL2* in the entry vector was
444 cloned into the destination vector, pGWB434. These constructs were transformed
445 into Col-0 plants by the floral dip method (Clough et al., 1998). All genotypes used
446 in this study were in the Columbia background. Plants were grown on
447 conventional half-strength Murashige and Skoog (1/2 MS) agar plates (pH 5.7) at
448 22°C under continuous light, unless stated otherwise.
449
450 **Vascular cell Induction culture System Using Arabidopsis Leaves (VISUAL)**
451 Plants were analysed using VISUAL as described previously (Kondo et al., 2016),
452 with a slight modification. Briefly, cotyledons of 6-day-old seedlings grown in
453 liquid 1/2 MS medium were cultured under continuous light in MS-based VISUAL
454 induction medium containing 0.25 mg/l 2,4-D, 1.25 mg/l kinetin, and 20 μM bikinin.
455 To observe ectopic xylem differentiation, a xylem indicator BF-170 (Sigma-
456 Aldrich) was added to the induction medium (Nurani et al., 2020). At 4 days after
457 induction, cotyledons were fixed in ethanol: acetic acid (3:1, v/v) and mounted
458 with a clearing solution (chloral hydrate: glycerol: water = 8:1:2 [w/w/v]). Images
459 obtained using a fluorescent stereomicroscope (M165, Laica) were binarized
460 using the “Threshold” function of the ImageJ software (Schneider et al., 2012).
461 Xylem differentiation ratio was calculated based on the BF-170 positive area cut-
462 off by suitable thresholding per a whole cotyledon area.
463
464 **Microarray Experiments**
465 To obtain the time-course maicroarray datasets, VISUAL was performed as
466 described above. After VISUAL induction, cultured cotyledons (6 to 10
467 cotyledons) were collected every six hours. Total RNA was extracted from
468 cultured cotyledons using an RNeasy Plant Mini Kit (Qiagen). Microarray
469 experiments were performed using the Arabidopsis Gene 1.0STArray
470 (Affymetrix) according to the standard Affymetrix protocol.
471
472 **Construction of the Coexpression Network**

473 Based on the VISUAL time-course maicroarray data, the VISUAL-induced genes
474 were defined as >8-fold changed genes compared with VISUAL for 0 and 72 h.
475 Median normalized values in log_2 scale of the VISUAL-induced genes (855
476 genes) were obtained from multiple transcriptome datasets: time-course, wild
477 type versus *bes1-1* (Saito et al. 2018), wild type versus *apl* (Kondo et al. 2016),
478 and SEOR1 cell-sorting data (Kondo et al. 2016). As described previously (Kondo
479 et al., 2016), the VISUAL coexpression network was constructed using the
480 weighted gene coexpression network analysis (WGCNA) package (Langfelder
481 and Horvath, 2008). The adjacency matrix was calculated with soft thresholding
482 power, which was chosen based on the criterion of scale-free topology (fit index
483 =0.8).
484
485 **Confocal laser scanning microscopy**
486 BF-170 signals in VISUAL samples were visualized using the FV1200 confocal
487 laser scanning microscope (Olympus). Z-series fluorescence images were
488 obtained at excitation and detection wavelengths of 473 and 490–540 nm,
489 respectively. Z-projection images were created using the ImageJ software.
490
491 **Quantitative reverse transcription PCR (qRT-PCR)**
492 Total RNA was extracted from cotyledons subjected to VISUAL experiments or
493 whole seedlings in other experiments using RNeasy Plant Mini Kit (Qiagen).
494 Quantitative PCR was performed using a LightCycler (Roche Diagnostics).
495 *UBQ14* (for VISUAL experiments) and *ACT2* (for other experiments) were used
496 as internal controls. Gene-specific primers and TaqMan Probe sets are listed in
497 Supplemental Table 4.
498
499 **RNA-seq**
500 Total RNA was extracted from cotyledons of Col-0 plants subjected to VISUAL
501 experiments (Kondo et al., 2015) at 0, 30, and 72 h after induction using RNeasy
502 Plant Mini Kit (Qiagen). RNA-seq analysis was carried out by Hokkaido System
503 Science Co., Ltd.

504

505 **Expression and purification of BES/BZR family proteins**

506 MBP-fused DNA-binding domains (DBDs) of BES1 (20T–103R) and BZR1 (21A–
507 104R) were expressed and purified as described previously (Nosaki et al., 2018).
508 The DBDs of BEH3 (4G–88S) and BEH4 (4G–89T) were cloned into pMAL-c2X
509 (New England Biolabs) and subsequently transformed into *Escherichia coli*
510 Rosetta (DE3) cells (Novagen). MBP-fused DBDs of BEH3 and BEH4 were
511 expressed and purified in the same way as BES1 and BZR1.

512

513 **Analysis of BES/BZR proteins by size exclusion chromatography (SEC)**

514 The purified proteins were loaded onto a Superdex 200 GL 10/300 (GE
515 Healthcare) column and eluted with a buffer containing 20 mM Tris-HCl (pH 7.5),
516 250 mM NaCl, 1 mM DTT, and 5% glycerol. To estimate the multimerization state
517 of BES/BZR family proteins, the following standards were used: thyroglobulin (*Mr*
518 670,000), bovine globulin (*Mr* 158,000), chicken ovalbumin (*Mr* 44,000), equine
519 myoglobin (*Mr* 17,000), and vitamin B-12 (*Mr* 1,350) (Bio-Rad).

520

521 **EMSA**

522 EMSAs of BES/BZR family proteins were performed as described previously
523 (Nosaki et al., 2018).

524

525 **Luciferase (LUC) assay**

526 Coding sequences (CDSs) of *BES1-L* (*At1g19350.3*), *BZR1* (*At1g75080.1*), and
527 *BEH4* (*At1g78700.1*) were cloned and fused to the ligand-binding domain of the
528 rat glucocorticoid receptor (GR). An approximately 1,952 bp sequence upstream
529 of the *DWF4* transcription start site was cloned and fused to ELUC with the PEST
530 domain (Tamaki et al., 2020) (Toyobo). *Rhizobium radiobacter* GV3101 MP90
531 strain harboring both effector and reporter constructs as well as a p19k
532 suppressor construct was infiltrated into *Nicotiana benthamiana* leaves. After 2
533 days, leaf discs excised from the transformed leaves were incubated with 200 μM
534 D-luciferin (Wako) for 2 h in white 24-well plates (PerkinElmer). Then, 10 μM

535 dexamethasone (DEX) was added into each well, and LUC activity was
536 measured using the TriStar2 LB942 (Berthold) system, as described previously
537 (Tamaki et al., 2020).
538
539 **Histological analysis**
540 Cross-sections of hypocotyls of seedlings were prepared as described previously
541 (Kondo et al., 2014). Samples were fixed in FAA solution containing 40% (v/v)
542 ethanol, 2.5% (v/v) acetic acid, and 2.5% (v/v) formalin. The fixed samples were
543 gradually dehydrated using an ethanol dilution series and then embedded in
544 Technovit 7100 resin (Kulzer). Sections of 5 μm thickness were prepared using
545 the RM2165 microtome (Leica). Sliced samples were stained with 0.1% (w/v)
546 toluidine blue for 1 min.
547
548 **Mathematical modeling**
549 A mathematical model for the competitive binding between BEH3 and other
550 homologs was constructed based on the assumptions that 1) there are *n* binding
551 sites at the promoter, and 2) the weak-type BEH3 is competitively superior to the
552 strong-type homologs in terms of binding to the promoter. The weak-type BEH3
553 occupies the vacant sites first, followed by the strong-type homologs, which
554 occupy the remaining vacant sites. The binding probabilities of the weak-type
555 BEH3 and strong-type homologs (p_{BEH3} and p_O, respectively) are proportional
556 to the transcript abundance of *BEH3* and other homologs, respectively. Using
557 p_{BEH3} and p_O, the probability that *i* BEH3 and *j* homologs bind to the promoter is
558 given as the product of two binomial distributions as follows:

559 $$f(i,j|p_{BEH3},p_O,n) = \binom{n}{i} p_{BEH3}^{i}(1-p_{BEH3})^{n-i} \times \binom{n-i}{j} p_O^{j}(1-p_O)^{n-i-j}.$$

560 Binding of BEH3 and other homologs to the binding sites suppresses the
561 transcription level of direct target genes leading to the repression of the
562 proliferation of stem cells. The effect of the binding sites of BEH3 and other
563 homologs on the cell proliferation rate of stem cells was designated as α and β,
564 respectively. Because the effect of BEH3 is weaker than that of other homologs,
565 $\alpha < \beta$ always holds. When *i* BEH3 and *j* homologs bind to the promoter, the cell

proliferation rate is given as $\alpha^i\beta^j$. The cell division rate should be proportional to the area inside the cambium, which was measured in experiments because the area inside the cambium increases with the increase in the rate of cell division. When there are multiple individuals, the expected rate of cell division of stem cell is calculated as follows:

$$E[cell\ division\ rate] = \sum_{i=0}^{n}\sum_{j=0}^{n-i}\alpha^i\beta^j f(i,j|p_{BEH3},p_O,n)$$

$$= [\alpha p_{BEH3} + (1-p_{BEH3})(\beta p_O + 1 - p_O)]^n$$

(1)

Using Equation (1), the variance of cell division rate can be calculated as:

$$V[cell\ division\ rate] = [\alpha^2 p_{BEH3} + (1-p_{BEH3})(\beta^2 p_O + 1 - p_O)]^n - [\alpha p_{BEH3} + (1-p_{BEH3})(\beta p_O + 1 - p_O)]^{2n}$$

(2)

The coefficient of variation (CV) of the cell division rate was calculated as:

$$CV = \sqrt{V[cell\ dividion\ rate]}/E[cell\ division\ rate]$$

Data availability

All data is available in the manuscript or the supplementary materials. All sequence reads were deposited in the NCBI Sequence Read Archive (SRA) database under the following accession numbers: XXXXXXX

AUTHER CONTRIBUTIONS

T.F., M.S., and Y.K. designed the experiments, coordinated the project, and wrote the manuscript; T.F, M.S., H.U., S.S., W.Y., S.N., T.M., and Y.K. performed the experiments; A.S. performed mathematical model simulations; M.T. and H.F. participated in discussions. All authors reviewed and edited the manuscript.

ACKNOWLEDGMENTS

We thank Yasuko Ozawa, Yuki Fukaya, and Akiho Suizu for technical support. We also thank Dr. Keiko U. Torii (University of Texas, Austin, Texas) for critically reading the manuscript and providing insightful comments. This work was funded by the Ministry of Education, Culture, Sports, Science and Technology, Japan (Scientific Research on Priority Areas and Scientific Research on Innovative Areas) (17H06476 and 20H05407 to Y.K., and 19H04855 to T.M.), and by the Japan Society for the Promotion of Science (17H05008 and 20K15815 to Y.K., 18H06065 and 20K15813 to T.F., 16H06377 to H.F., 19K23658 to S.N., and 18KK0170 and 18H02185 to W.Y.).

REFERENCES

Shi, D., Tavhelidse, T. Thumberger, T., Wittbrodt, J., and Greb, T. (2017). Bifacial stem cell niches in fish and plants. Curr. Opin. Genet. Dev. **45**: 28-33.

De Rybel, B., Mähönen, A. P., Helariutta, Y., and Weijers, D. (2016). Plant vascular development: from early specification to differentiation. Nat. Rev. Mol. Cell Biol. **17**: 30–40.

Fischer, U., Kucukoglu, M., Helariutta, Y., and Bhalerao, R. P. (2019). The Dynamics of Cambial Stem Cell Activity. Annu. Rev. Plant Biol. **70**: 293–319.

Ito, Y., Nakanomyo, I., Motose, H., Iwamoto, K., Sawa, S., Dohmae, N., and Fukuda, H. (2006). Dodeca-CLE peptides as suppressors of plant stem cell differentiation. Science **313**: 842–845.

Fisher, K., and Turner, S. (2007). PXY, a receptor-like kinase essential for maintaining polarity during plant vascular-tissue development. Curr. Biol. **17**: 1061–1066.

Hirakawa, Y., Shinohara, H., Kondo, Y., Inoue, A., Nakanomyo, I., Ogawa, M., Sawa, S., Ohashi-Ito, K., Matsubayashi, Y., and Fukuda, H. (2008). Non-cell-autonomous control of vascular stem cell fate by a CLE peptide/receptor system. Proc. Natl. Acad. Sci. USA. **105**: 15208–15213.

Hirakawa, Y., Kondo, Y.,and Fukuda, H. (2010). TDIF peptide signaling regulates vascular stem cell proliferation via the WOX4 homeobox gene in Arabidopsis. Plant cell **22**: 2618–2629.

Etchells, J. P., and Turner, S. R. (2010). The PXY-CLE41 receptor ligand pair defines a multifunctional pathway that controls the rate and orientation of vascular cell division. Development **137**: 767–774.

Han, S., Cho, H., Noh, J., Qi, J., Jung, H. J., Nam, H., Lee, S., Hwang, D., Greb, T., and Hwang, I. (2018). BIL1-mediated MP phosphorylation integrates PXY and cytokinin signalling in secondary growth. Nat. plants **4**: 605–614.

Etchells, J. P., Provost, C. M., and Turner, S. R. (2012). Plant vascular cell division is maintained by an interaction between PXY and ethylene signalling. PLoS Genet. **8**: e1002997.

Kondo, Y., and Fukuda, H. (2015). The TDIF signaling network. Curr. Opin. Plant Biol. **28**: 106–110.

Zhang, J., Eswaran, G., Alonso-Serra, J., Kucukoglu, M., Xiang, J., Yang, W., Elo, A., Nieminen, K., Damén, T., Joung, J. G., Yun, J. Y., Lee, J. H., Ragni, L., Barbier de Reuille, P., Ahnert, S. E., Lee, J. Y., Mähönen, A. P., and Helariutta, Y. (2019). Transcriptional regulatory framework for vascular cambium development in Arabidopsis roots. Nat. plants **5**: 1033–1042.

Shi, D., Jouannet, V., Agustí, J., Kaul, V., Levitsky, V., Sanchez, P., Mironova, V. V., and Greb, T. (2020). Tissue-specific transcriptome profiling of the Arabidopsis inflorescence stem reveals local cellular signatures, The Plant Cell, koaa019, https://doi.org/10.1093/plcell/koaa019

Kondo Y. (2018). Reconstitutive approach for investigating plant vascular development. J. Plant Res. **131**: 23–29.

Kondo, Y., Nurani, A. M., Saito, C., Ichihashi, Y., Saito, M., Yamazaki, K., Mitsuda, N., Ohme-Takagi, M., and Fukuda, H. (2016). Vascular Cell Induction Culture System Using Arabidopsis Leaves (VISUAL) Reveals the Sequential Differentiation of Sieve Element-Like Cells. Plant cell **28**: 1250-1262.

Kondo, Y., Ito, T., Nakagami, H., Hirakawa, Y., Saito, M., Tamaki, T., Shirasu, K., and Fukuda, H. (2014). Plant GSK3 proteins regulate xylem cell differentiation downstream of TDIF-TDR signalling. Nat. Commun. **24**: 3504.

Saito, M., Kondo, Y., and Fukuda, H. (2018). BES1 and BZR1 Redundantly Promote Phloem and Xylem Differentiation. Plant Cell Physiol. **59**: 590-600.

Kondo, Y., Fujita, T., Sugiyama, M., and Fukuda, H. (2015). A novel system for xylem cell differentiation in *Arabidopsis thaliana*. Mol. Plant **8**: 612-621.

Brady, S. M., Orlando, D. A., Lee, J. Y., Wang, J. Y., Koch, J., Dinneny, J. R., Mace, D., Ohler, U., and Benfey, P. N. (2007). A high-resolution root spatiotemporal map reveals dominant expression patterns. Science **318**: 801-806.

Shi, D., Lebovka, I., López-Salmerón, V., Sanchez, P., and Greb, T. (2019). Bifacial cambium stem cells generate xylem and phloem during radial plant growth. Development **146**: dev171355

686

687 **Randall, R. S., Miyashima, S., Blomster, T., Zhang, J., Elo, A., Karlberg, A.,**
688 **Immanen, J., Nieminen, K., Lee, J. Y., Kakimoto, T., Blajecka, K., Melnyk, C.**
689 **W., Alcasabas, A., Forzani, C., Matsumoto-Kitano, M., Mähönen, A. P.,**
690 **Bhalerao, R., Dewitte, W., Helariutta, Y., Murray, J. A.** (2015).
691 AINTEGUMENTA and the D-type cyclin CYCD3;1 regulate root secondary
692 growth and respond to cytokinins. Biol Open. **4**: 1229-36.

693

694 **Smit, M. E., McGregor, S. R., Sun, H., Gough, C., Bågman, A. M., Soyars, C.**
695 **L., Kroon, J. T., Gaudinier, A., Williams, C. J., Yang, X., Nimchuk, Z. L.,**
696 **Weijers, D., Turner, S. R., Brady, S. M., and Etchells, J. P.** (2020). A PXY-
697 Mediated Transcriptional Network Integrates Signaling Mechanisms to Control
698 Vascular Development in Arabidopsis. Plant Cell. **32**: 319-335.

699

700 **Lachowiec, J., Mason, G. A., Schultz, K., and Queitsch, C.** (2018).
701 Redundancy, Feedback, and Robustness in the *Arabidopsis thaliana BZR/BEH*
702 Gene Family. Front. Genet. **9**: 523.

703

704 **Feltz, C. J., and Miller, G. E.** (1996). An asymptotic test for the equality of
705 coefficients of variation from k population. Stat. Med. **15**: 647–658.

706

707 **Krishnamoorthy, K., and Lee, M.** (2014). Improved tests for the equality of
708 normal coefficients of variation. Comput. Stat. **29**: 215–232.

709

710 **Yin, Y., Vafeados, D., Tao, Y., Yoshida, S., Asami, T., and Chory, J.** (2005). A
711 new class of transcription factors mediates brassinosteroid-regulated gene
712 expression in *Arabidopsis*. Cell **120**: 249-259.

713

714 **Chen, L. G., Gao, Z., Zhao, Z., Liu, X., Li, Y., Zhang, Y., Liu, X., Sun, Y., and**
715 **Tang, W.** (2019a). BZR1 Family Transcription Factors Function Redundantly and

716 Indispensably in BR Signaling but Exhibit BRI1-Independent Function in
717 Regulating Anther Development in *Arabidopsis*. Mol. Plant **12**: 1408-1415.
718
719 **Chen W, Lv M, Wang Y, Wang PA, Cui Y, Li M, Wang R, Gou X, and Li J.**
720 (2019b). BES1 is activated by EMS1-TPD1-SERK1/2-mediated signaling to
721 control tapetum development in *Arabidopsis thaliana*. Nat. Commun. **10**: 4164.
722
723 **Nolan, T. M., Vukašinović, N., Liu, D., Russinova, E., and Yin, Y.** (2020).
724 Brassinosteroids: Multidimensional Regulators of Plant Growth, Development,
725 and Stress Responses. Plant Cell **32**: 295-318.
726
727 **Nurani, A. M., Ozawa, Y., Furuya, T., Sakamoto, Y., Ebine, K., Matsunaga, S.,**
728 **Ueda, T., Fukuda, H., and Kondo, Y.** (2020). Deep Imaging Analysis in VISUAL
729 Reveals the Role of YABBY Genes in Vascular Stem Cell Fate Determination.
730 Plant Cell Physiol. **61**: 255-264.
731
732 **Yin, Y., Wang, Z. Y., Mora-Garcia, S., Li, J., Yoshida, S., Asami, T., and Chory,**
733 **J.** (2002). BES1 accumulates in the nucleus in response to brassinosteroids to
734 regulate gene expression and promote stem elongation. Cell **109**: 181–191.
735
736 **Wang, Z. Y., Nakano, T., Gendron, J., He, J., Chen, M., Vafeados, D., Yang,**
737 **Y., Fujioka, S., Yoshida, S., Asami, T., and Chory, J.** (2002). Nuclear-localized
738 BZR1 mediates brassinosteroid-induced growth and feedback suppression of
739 brassinosteroid biosynthesis. Dev. Cell **2**: 505–513.
740
741 **Oh, E., Zhu, J. Y., Ryu, H., Hwang, I., and Wang, Z. Y.** (2014). TOPLESS
742 mediates brassinosteroid-induced transcriptional repression through interaction
743 with BZR1. Nat. commun. **5**: 4140.
744

745 **He, J. X., Gendron, J. M., Sun, Y., Gampala, S. S., Gendron, N., Sun, C. Q.,**
746 **and Wang, Z. Y.** (2005). BZR1 is a transcriptional repressor with dual roles in
747 brassinosteroid homeostasis and growth responses. Science **307**: 1634-1638.
748
749 **Sun, Y., Fan, X. Y., Cao, D. M., Tang, W., He, K., Zhu, J. Y., He, J. X., Bai, M.**
750 **Y., Zhu, S., Oh, E., Patil, S., Kim, T. W., Ji, H., Wong, W. H., Rhee, S. Y., and**
751 **Wang, Z. Y.** (2010). Integration of brassinosteroid signal transduction with the
752 transcription network for plant growth regulation in *Arabidopsis*. Dev. Cell **19**:
753 765–777.
754
755 **Yu, X., Li, L., Zola, J., Aluru, M., Ye, H., Foudree, A., Guo, H., Anderson, S.,**
756 **Aluru, S., Liu, P., Rodermel, S., and Yin, Y.** (2011). A brassinosteroid
757 transcriptional network revealed by genome-wide identification of BESI target
758 genes in *Arabidopsis thaliana*. Plant J. **65**: 634–646.
759
760 **Chung, Y., Maharjan, P. M., Lee, O., Fujioka, S., Jang, S., Kim, B., Takatsuto,**
761 **S., Tsujimoto, M., Kim, H., Cho, S., Park, T., Cho, H., Hwang, I., and Choe, S.**
762 (2011). Auxin stimulates *DWARF4* expression and brassinosteroid biosynthesis
763 in Arabidopsis. Plant J. **66**: 564–578.
764
765 **Nosaki, S., Miyakawa, T., Xu, Y., Nakamura, A., Hirabayashi, K., Asami, T.,**
766 **Nakano, T., and Tanokura, M.** (2018). Structural basis for brassinosteroid
767 response by BIL1/BZR1. Nat. Plants **4**: 771-776.
768
769 **Aoyama, T., Dong, C. H., Wu, Y., Carabelli, M., Sessa, G., Ruberti, I., Morelli,**
770 **G., and Chua, N. H.** (1995). Ectopic expression of the Arabidopsis transcriptional
771 activator Athb-1 alters leaf cell fate in tobacco. Plant Cell **7**: 1773–1785.
772
773 **Oh, E., Zhu, J. Y,. and Wang, Z. Y.** (2012). Interaction between BZR1 and PIF4
774 integrates brassinosteroid and environmental responses. Nat. Cell Biol. **14**: 802–
775 809.

776

777 **Deng, T., and Karin, M.** (1993). JunB differs from c-Jun in its DNA-binding and
778 dimerization domains, and represses c-Jun by formation of inactive heterodimers.
779 Genes Dev. **7**: 479-490.

780

781 **Jiang, J., Zhang, C., and Wang, X.** (2015). A recently evolved isoform of the
782 transcription factor BES1 promotes brassinosteroid signaling and development
783 in *Arabidopsis thaliana*. Plant Cell **27**: 361–374.

784

785 **Tsutsui, H., and Higashiyama, T.** (2017). pKAMA-ITACHI Vectors for Highly
786 Efficient CRISPR/Cas9-Mediated Gene Knockout in Arabidopsis thaliana. Plant
787 Cell Physiol. **58**: 46-56.

788

789 **Ohashi-Ito, K., Oda, Y., and Fukuda, H.** (2010). *Arabidopsis* VASCULAR-
790 RELATED NAC-DOMAIN6 directly regulates the genes that govern programmed
791 cell death and secondary wall formation during xylem differentiation. Plant Cell
792 **22**: 3461-3473.

793

794 **Clough, S. J., and Bent, A. F.** (1998). Floral dip: a simplified method for
795 *Agrobacterium*-mediated transformation of *Arabidopsis thaliana*. Plant J. **16**: 735-
796 743.

797

798 **Schneider, C. A., Rasband, W. S., and Eliceiri, K. W.** (2012). NIH Image to
799 ImageJ: 25 years of image analysis. Nat. Methods **9**: 671–675.

800

801 **Langfelder, P., and Horvath, S.** (2008). WGCNA: an R package for weighted
802 correlation network analysis. BMC bioinformatics **9**: 559.

803

804 **Tamaki, T., Oya, S., Naito, M., Ozawa, Y., Furuya, T., Saito, M., Sato, M.,**
805 **Wakazaki, M., Toyooka, K., Fukuda, H., Helariutta, Y., and Kondo Y.** (2020).

806 VISUAL-CC system uncovers the role of GSK3 as an orchestrator of vascular cell
807 type ratio in plants. Commun. Biol. 3: 184.

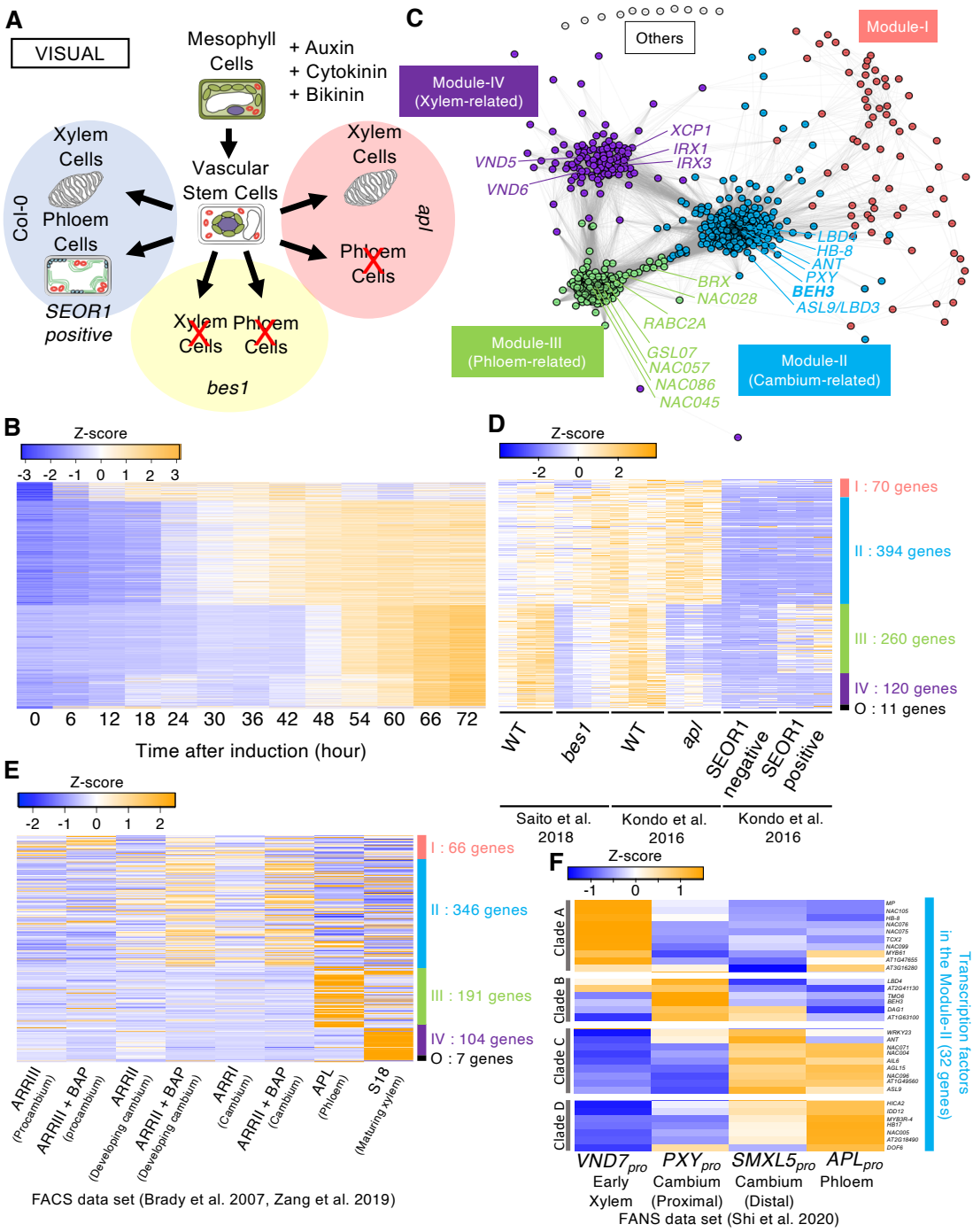

Figure 1. Classification of the VISUAL-induced genes based on the gene coexpression network analysis

(A) Schematic showing the transdifferentiation process in Col-0 (WT, left), *bes1* mutants (lower), and *apl* mutants (right).

813 **(B)** Expression profiles of the VISUAL-induced genes in the VISUAL time-course
814 microarray data. The VISUAL-induced genes were defined as >8-fold changed
815 genes when compared VISUAL at 0 and 72 h. Expression was visualized with a
816 heat map image according to Z score according to their expression levels. Color
817 bars in the right side indicates each module in accordance with (C).
818 **(C)** Coexpression network of the VISUAL-induced genes using the WGCNA
819 package. Four distinct modules are highlighted with different colors. A node
820 represents a gene. An edge indicates high correlation between nodes (TOM >
821 0.02).
822 **(D)** Expression profiles of the VISUAL-induced genes in the multiple VISUAL
823 microarray datasets. VISUAL microarray datasets were provided from each
824 comparison between WT and *bes1-1* (Saito et al. 2018), WT and *apl* (Kondo et
825 al. 2016), and SEOR1-negative and SEOR1-positive cells (Kondo et al. 2016).
826 **(E)** Expression profiles of the VISUAL-induced genes in the FACS dataset (Bardy
827 et al., 2007, Zang et al., 2019).
828 **(F)** Expression profiles of the cambium-related genes (Module-II) in the FANS
829 dataset (Shi et al., 2020). The gene names are shown on the right side.
830

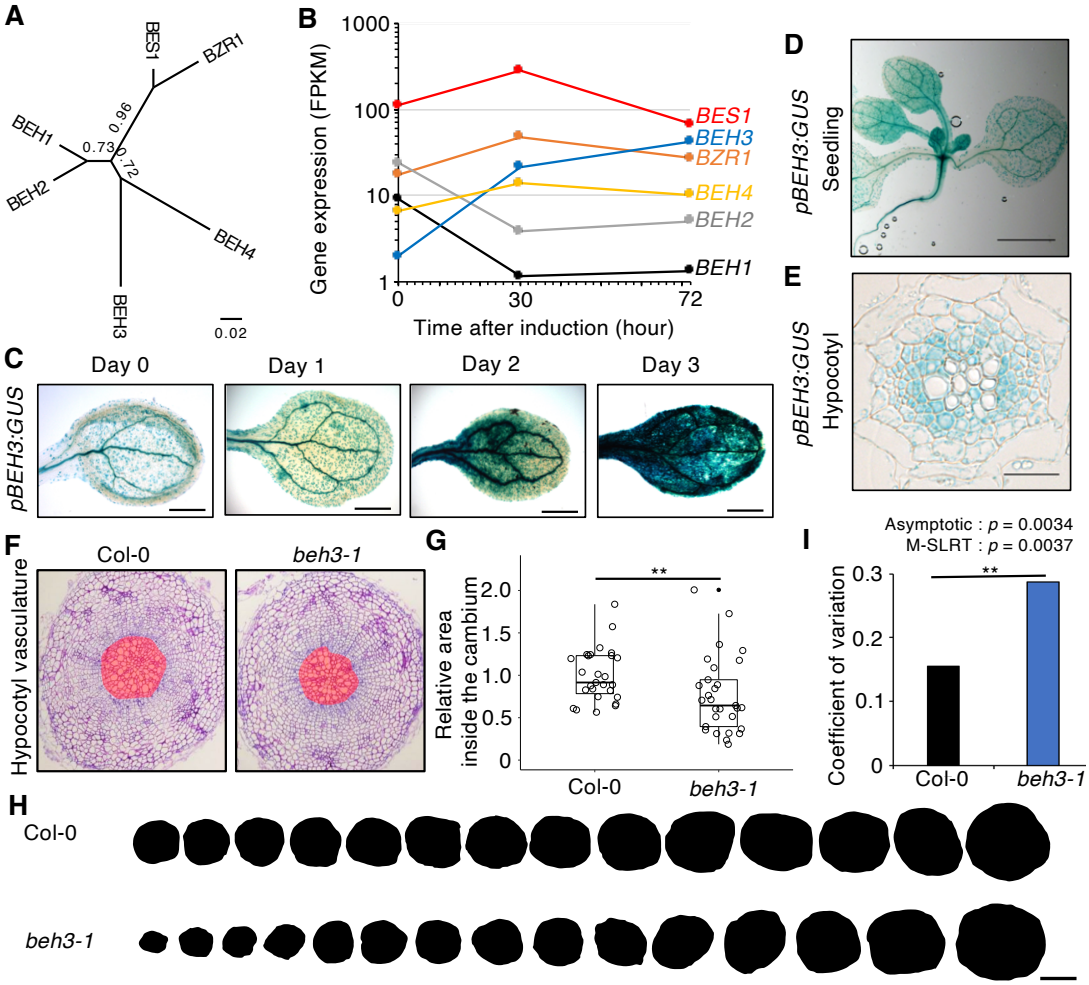

Figure 2. BEH3 provides the stability for secondary growth in the cambium

(A) An unrooted phylogenetic tree of Arabidopsis BES/BZR family members.

(B) Time-course expression analysis of BES1 homologs genes using VISUAL. Gene expression levels at each time point were analyzed by RNA-seq.

(C-E) GUS activity in *pBEH3:GUS* transgenic plants. GUS staining was performed using cotyledons subjected to VISUAL (C) shoot of 20-day-old seedling (D) and hypocotyl section of 7-day-old seedling (E).

(F) Sections of hypocotyl vasculature of WT and *beh3-1* mutant plants grown under short-day conditions for 21 days.

(G) Relative areas inside the cambium were calculated in comparison with the mean value of the WT (**$P < 0.01$; Student's *t*-test, $n = 28$ [WT], 30 [*beh3-1*]).

843 **(H)** Size variation inside the cambium of WT and *beh3* plants. Black circles
844 indicate areas inside the cambium of each individual for the odd number samples
845 in ascending order of (F).
846 **(I)** CV of the areas inside the cambium of WT and *beh3* plants. Statistical analysis
847 of differences between the WT and *beh3* mutants using Asymptotic and M-
848 SLART.
849 Scale bars = 1 mm (C), 2 mm (D), and 100 μm (E,F,I).
850

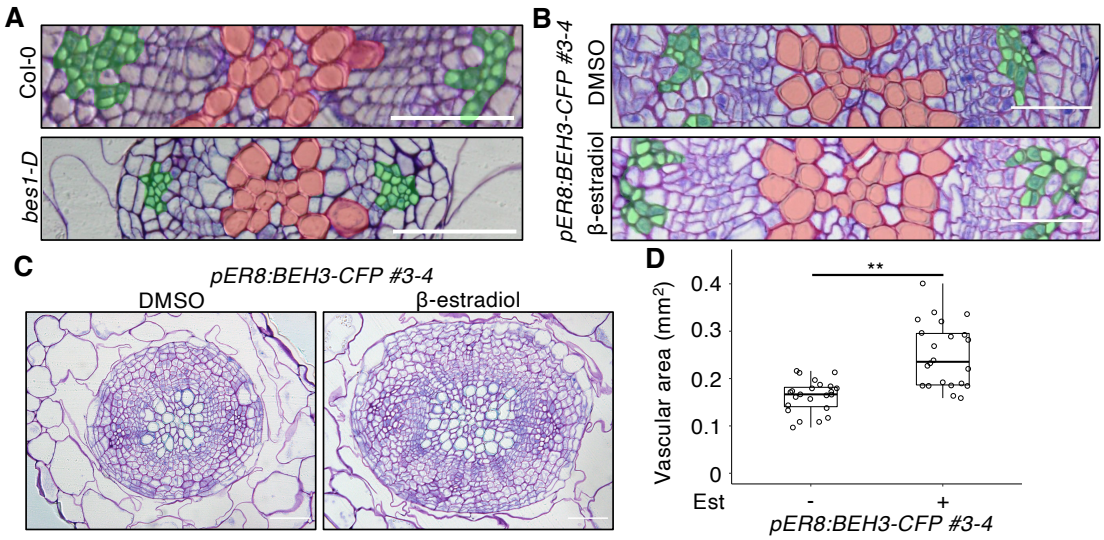

Figure 3. BEH3 overexpression promotes secondary growth

(A) Sections of hypocotyl vasculature of 11-day-old WT and *bes1-D* seedlings. Red and green area indicates xylem cells and phloem cells, respectively.

(B-C) Sections of hypocotyl vasculature of β-estradiol-inducible BEH3-overexpressing plants treated with (+) or without (-) 5 μM β-estradiol for 12 days. Red and green area in (B) indicate xylem cells and phloem cells, respectively.

(D) Calculated vascular areas in (C) are shown using box-and-whisker plots. White circles indicate values of each sample (**P* < 0.05, ***P* < 0.01; Student's *t*-test; *n* = 23).

Scale bars = 100 μm (A–C).

Fig. 4

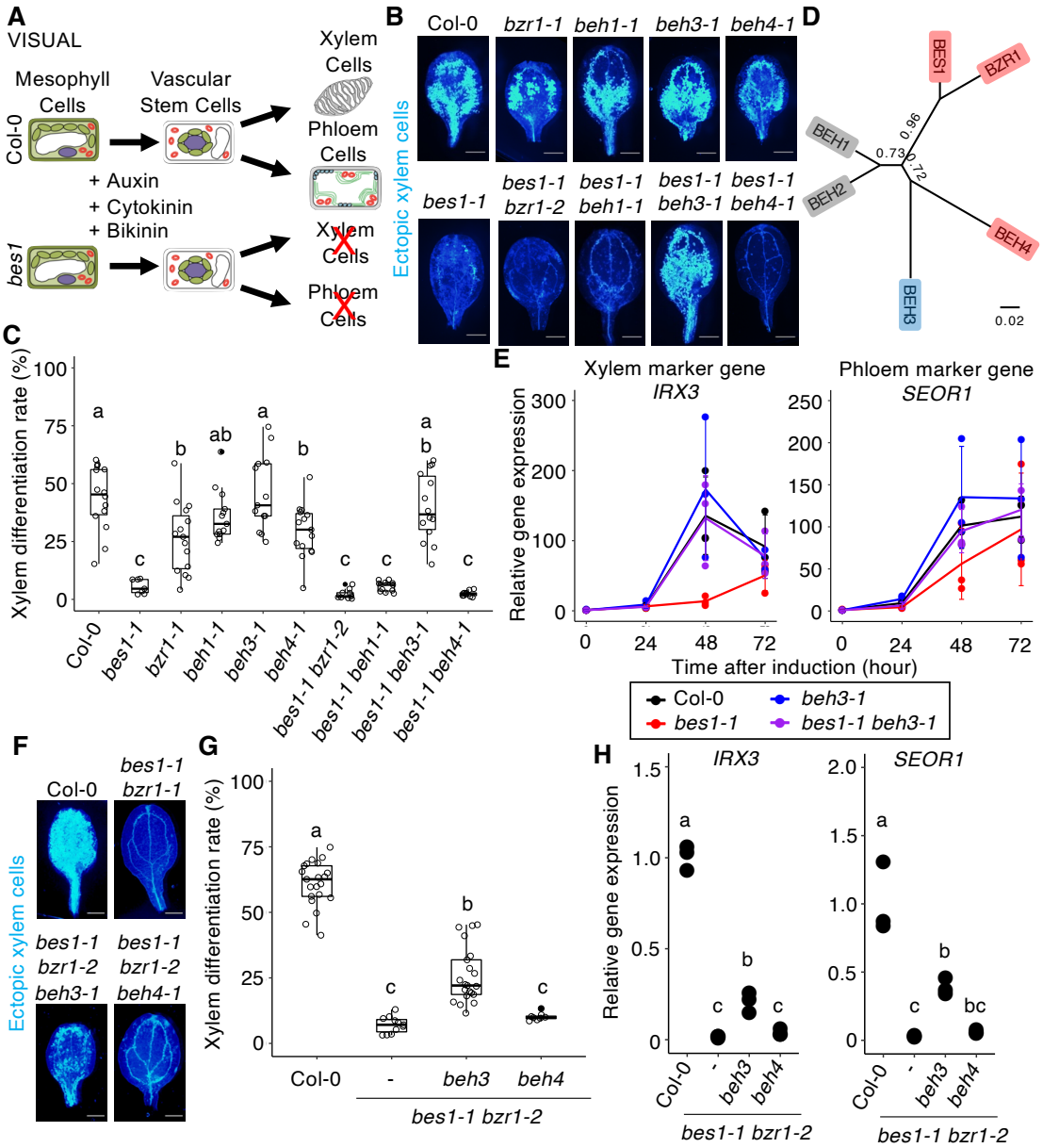

Figure 4. BEH3 antagonistically functions against BES1 and BZR1 in VISUAL

(A) Schematic showing the transdifferentiation process in Col-0 (WT, upper) and *bes1* mutants (lower).

(B, C) Ectopic xylem cell differentiation ratio in a combination of *bes/bzr* mutants. Bright blue signal in (B) indicates xylem cell wall stained with BF-170. Quantified xylem differentiation ratio is shown using box-and-whisker plots in (C). White

871 circles indicate the xylem differentiation ratio for each sample. Different letters
872 indicate significant differences ($P < 0.05$; Tukey-Kramer test).
873 **(D)** Effects of BES/BZR family members toward vascular cell differentiation in
874 VISUAL. Red, blue, and grey indicate “promote”, “suppress”, and “no effect”,
875 respectively.
876 **(E)** Time-course expression analysis of xylem-specific (*IRX3*) and phloem-
877 specific (*SEOR1*) marker genes. Relative fold changes were calculated in
878 comparison with the WT at 0 h after induction. Data represent mean ± standard
879 deviation (SD; n = 3). Results of two-way analysis of variance (ANOVA) are
880 summarized in Supplemental Table 1.
881 **(F, G)** Ectopic xylem differentiation in triple mutants. Bright blue signal in (F)
882 indicates xylem cell wall stained with BF-170. Xylem differentiation ratio is shown
883 using box-and-whisker plots in (G).
884 **(H)** Expression levels of *IRX3* and *SEOR1* in triple mutants at 48 h after induction.
885 Relative fold changes were calculated in comparison with the WT at 0 h after
886 induction ($n = 3$). Different letters indicate significant differences ($P < 0.05$; Tukey-
887 Kramer test).
888 Scale bars = 1 cm in (B,F).

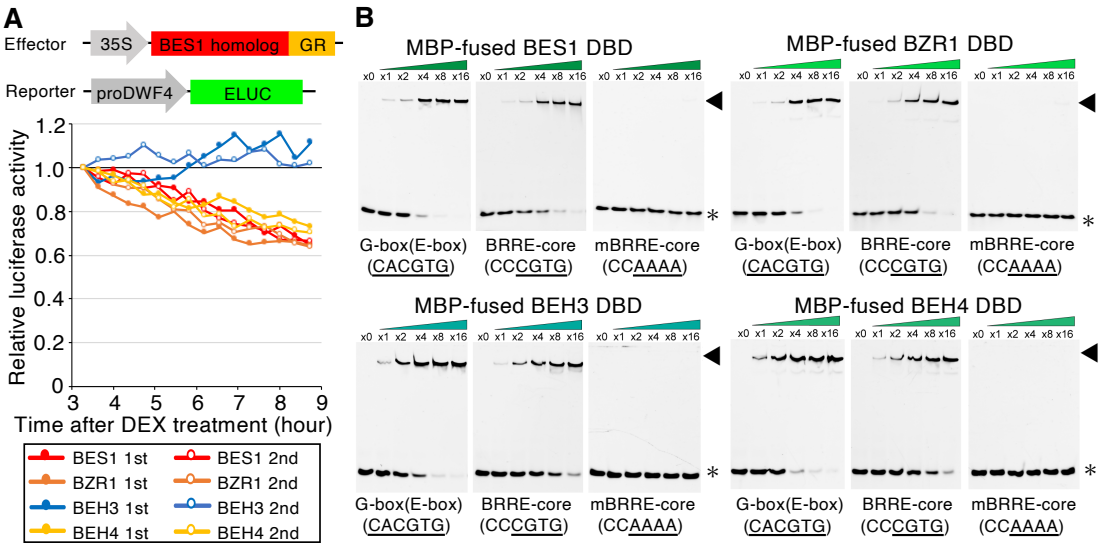

Figure 5. BEH3 competes with other BES/BZR homologs

(A) Transcriptional repressor activity of BES/BZR proteins in the *Nicotiana benthamiana* transient expression assay. Luciferase (LUC) activities in *pDWF4:ELUC* transgenic plants were calculated as average photon counts per second of six leaf disks and were normalized relative to values of DEX-treated samples harboring an empty effector construct.

(B) DNA-binding ability of BES/BZR proteins in the electrophoretic mobility shift assay (EMSA). Asterisks and arrowheads indicate the positions of free DNA and DNA-binding domain (DBD)-containing protein-bound DNA, respectively.

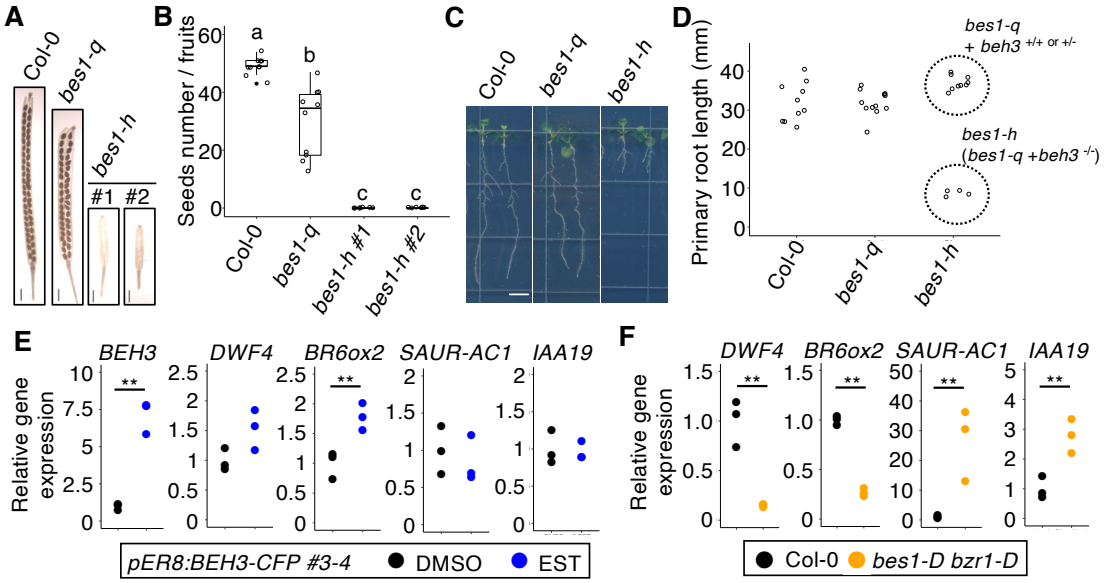

Figure 6. BEH3 passively inhibits the repressor activity of other BES/BZR homologs

(A, B) Development of fruits and seeds in *bes1* quintuple (*bes1-q*) and hextuple (*bes1-h*) mutants. Number of seeds in each mature fruit are shown using box-and-whisker plots in (B). Different letters indicate significant differences ($P < 0.05$; Tukey-Kramer test; $n = 10$).

(C, D) Primary root length in 11-day-old *bes1-q* and *bes1-h* mutant seedlings. To obtain homozygous *bes1-h* mutant plants, self-fertilized progenies of the T2 heterozygous *bes1-q* mutants, which containing $beh3^{+/-}$ mutation, were used. n = 10 (WT), 12 (*bes1-q*), and 13 (*bes1-h*).

(E) Expression levels of BES/BZR target genes in the estradiol-inducible BEH3 overexpression line. Eight-day-old seedlings were treated with 10 μM β-estradiol for 9h. Relative gene expression levels were calculated in comparison with the DMSO-treated sample (**$P < 0.01$; Student's *t*-test; $n = 3$).

(F) Expression level of BES/BZR target genes in *bes1-D bzr1-D*. Nine-day-old seedlings were used. Relative gene expression levels were calculated in comparison with the WT (**$P < 0.01$; Student's *t*-test; $n = 3$).

Scale bars = 1 mm (A and C).

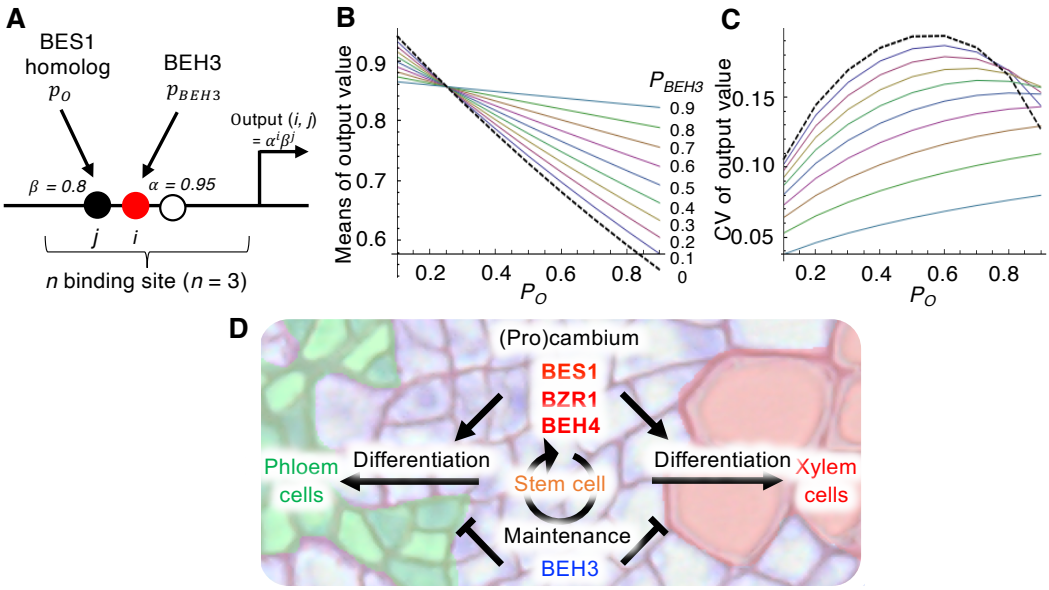

Figure 7. Competitive relationship among BES/BZR family provides the robustness for the control of vascular stem cell activity

(A) Schematic representation of the mathematical model that describes competitive binding between BEH3 and other homologs. BEH3 binds to i of n binding sites at a certain binding rate (P_{BEH3}). Then, other BES1 homologs (P_o) bind to *j* of *n-i* binding sites at a certain binding rate. Signaling output (*i*, *j*) is defined as $\alpha^i\beta^j$; α and β represent coefficients of transcriptional activity (<1 in the case of a repressor) of BEH3 and other BES1 homologs, respectively.

(B, C) Simulated signaling output when verifying both P_{BEH3} and P_o (n =3; α = 0.95; β = 0.8). Means and c oefficient of variation (CV) (CV = standard deviation/mean) of output values are shown in (B) and (C), respectively.

(D) Model showing the role of BES/BZR family members in the robust control of vascular stem cell differentiation and maintenance. Scale bars = 100 μm (H–J).

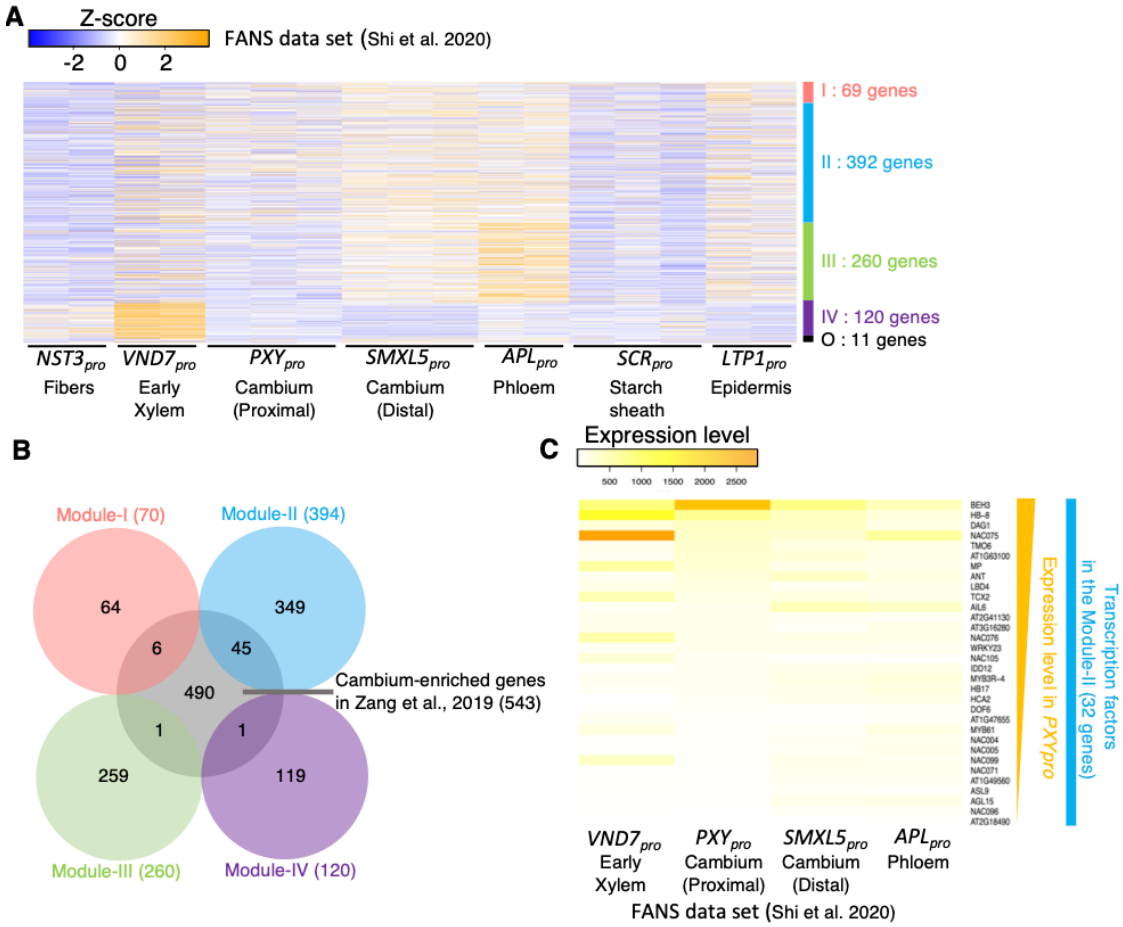

Supplemental Figure 1. Comprehensive analysis of the VISUAL coexpression network and vascular-related transcriptome datasets. (Supports Figure 1)

(A) Expression profiles of the VISUAL-induced genes in the FANS dataset (Shi et al., 2020).

(B) Venn diagram of genes in each module of the VISUAL-induced genes and the cambium-enriched genes (Zang et al., 2019).

(C) Expression levels of the cambium-related genes (Module-II) in the FANS dataset (Shi et al., 2020). The gene names are shown on the right side.

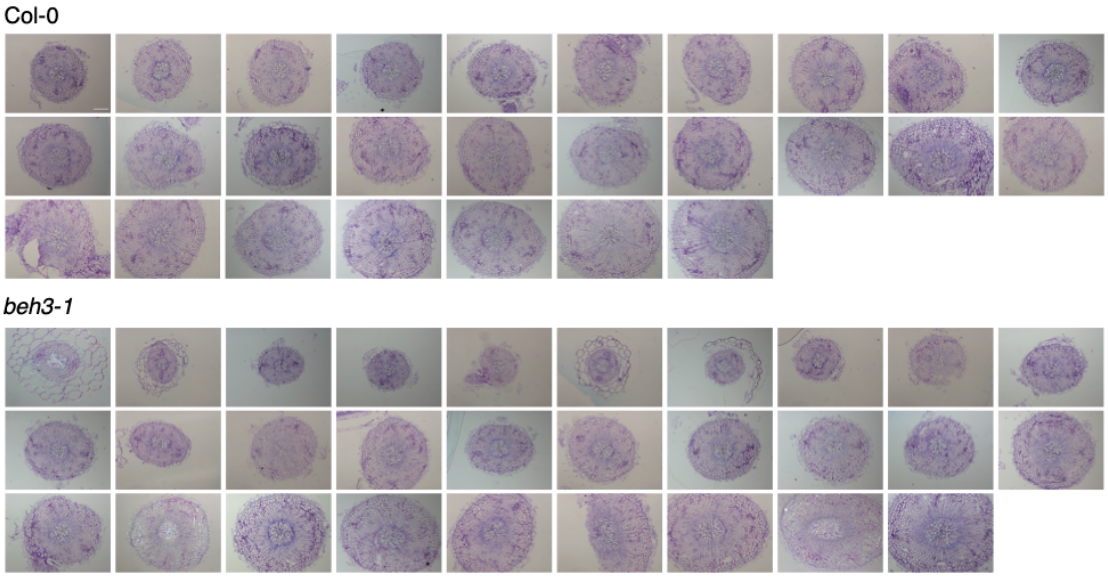

Supplemental Figure 2. All section images of hypocotyl vasculature of WT and *beh3-1* mutants. (Supports Figure 2)

All section images for Figure 2F. Sections of hypocotyl vasculature of WT and *beh3-1* mutants grown under short day conditions for 21 days. Scale bars = 100 µm.

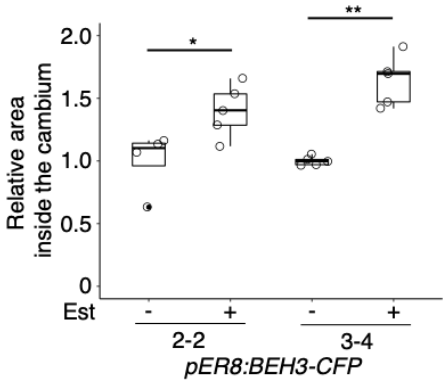

Supplemental Figure 3. Sections of hypocotyl vasculature of the β-estradiol inducible *BEH3*-overexpressing plants. (Supports Figure 3)

Plants were grown with or without 5 μM β-estradiol for 12 days. Relative areas inside the cambium were calculated in comparison with mean value of DMSO treated samples Quantified values were shown in box-and-whisker plots. White circles indicate the xylem differentiation ratio for each sample. (*$P < 0.05$ and **$P < 0.01$; Student's *t*-test).

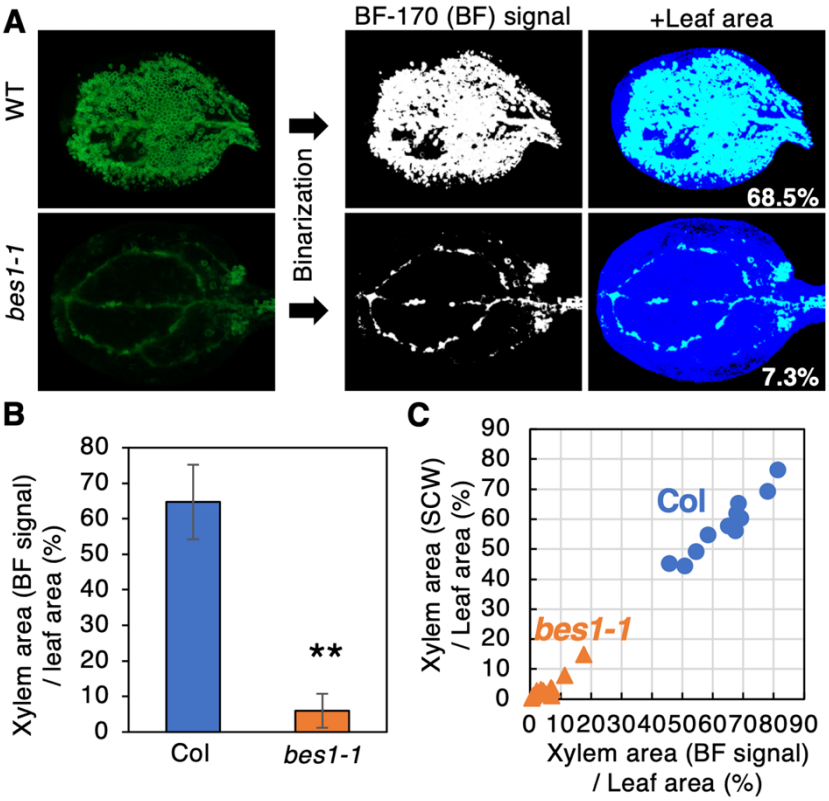

Supplemental Figure 4. Semi-automatic calculation of xylem differentiation ratio by the binarization method. (Supports Figure 4)

(A) The procedure of image thresholding in the WT and *bes1-1* after the VISUAL induction. The BF-170 signal (BF signal) area and the leaf area was shown by white and blue colour, respectively. The number written in the lower right represents the BF signal area per the leaf area (%) calculated by the binarization method.

(B) Xylem area calculated based on BF signal per leaf area (%) in the WT and *bes1-1*. Statistical differences were examined by Student's t-test (**$P < 0.005$). Error bars indicate SD ($n = 12$).

(C) Comparison of two calculation methods for xylem differentiation ratio. X axis indicates the ratio of xylem area calculated from BF signal per the leaf area. Y axis indicates the ratio of xylem area calculated from bright field images per the leaf area. There is a strong positive correlation between them.

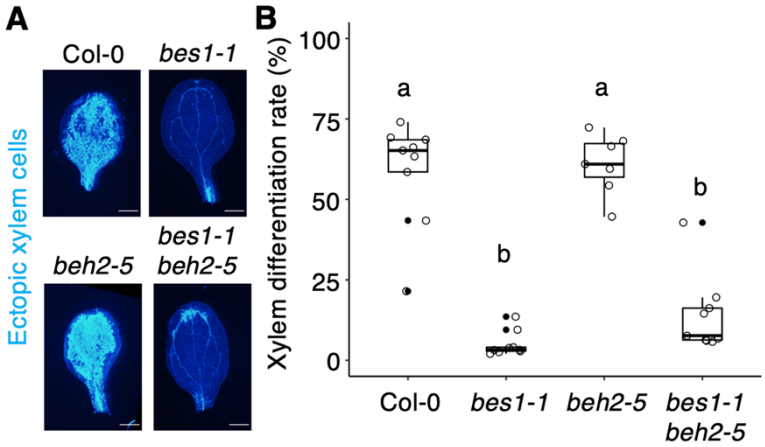

973

974 **Supplemental Figure 5. Ectopic xylem differentiation in VISUAL with *beh2***
975 **and *bes1 beh2* mutants.** (Supports Figure 4)
976 **(A)** A bright blue signal indicates xylem cell wall stained with BF-170.
977 **(B)** Quantified xylem differentiation ratio was shown by box-and-whisker plots.
978 White circles indicate the xylem differentiation ratio for each sample. Different
979 letters indicate significant differences ($P < 0.05$; Tukey-Kramer test).
980

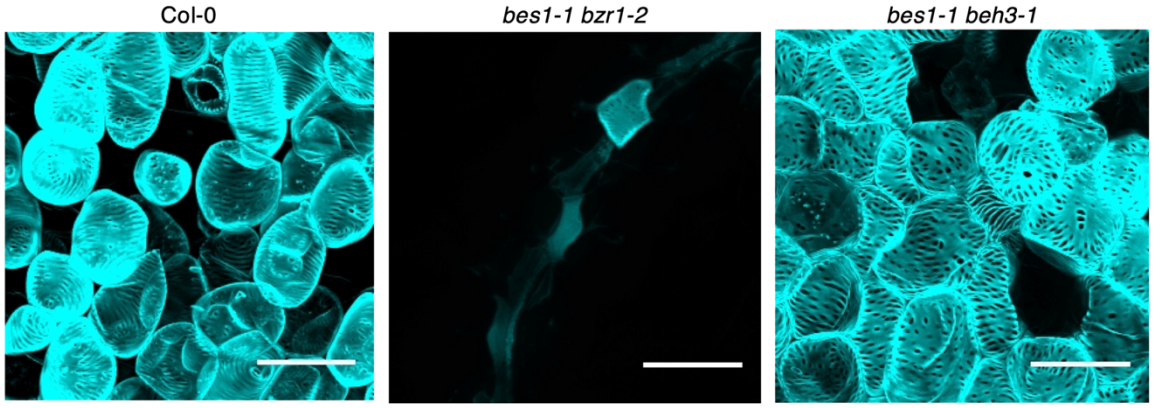

Supplemental Figure 6. Ectopic xylem cells in VISUAL observed using confocal laser scanning microscope. (Supports Figure 4)

Cotyledons of WT (Col-0), *bes1-1 bzr1-2*, and *bes1-1 beh3-1* were cultured with xylem indicator, BF170, for 4 days. A bright blue signal indicates BF170-incorporated xylem cell walls. Bars, 100 μm.

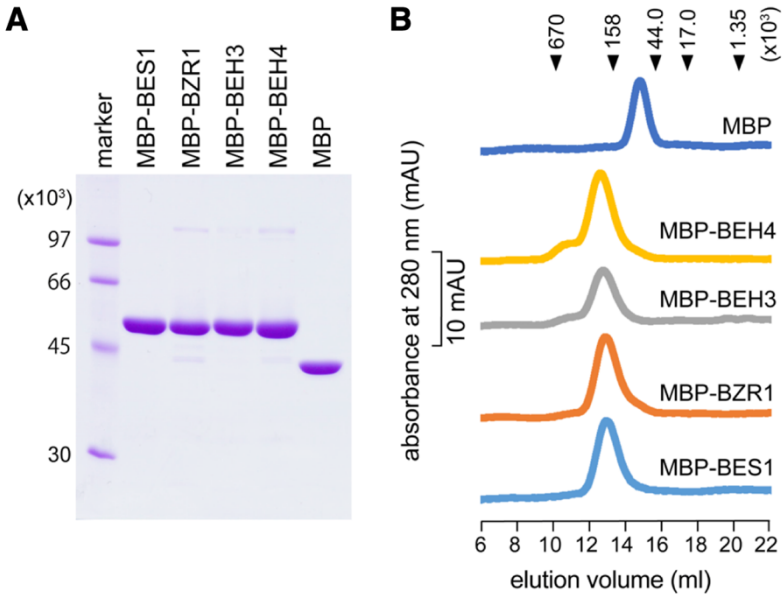

Supplemental Figure 7. Preparation of MBP-fused proteins of BES/BZR family DBDs for EMSA assay. (Supports Figure 5)

(A) Coomassie-stained SDS-PAGE analysis of the maltose-binding protein (MBP)-fused BES1, BZR1, BEH3 and BEH4 DBDs after purification.

(B) Oligomeric state analysis of MBP-fused BES1, BZR1, BEH3 and BEH4 DBDs by size exclusion chromatography (SEC). The peak positions of the marker proteins are indicated by the black triangles at the top of the chromatogram.

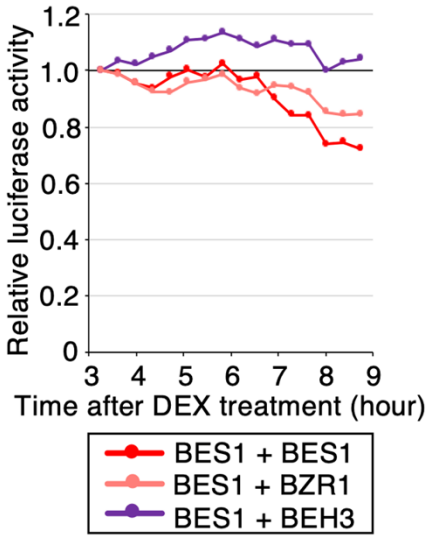

Supplemental Figure 8. Combinatory effects on transcriptional repressor activity in the *Nicotiana benthamiana* transient expression assay. (Supports Figure 5)

When *BZR1* or *BEH3* was co-expressed with *BES1*, luciferase (LUC) activities in *pDWF4:ELUC* transgenic plants were calculated as average photon counts per second of six leaf disks and were normalized relative to values of DEX-treated samples harbouring an empty effector construct.

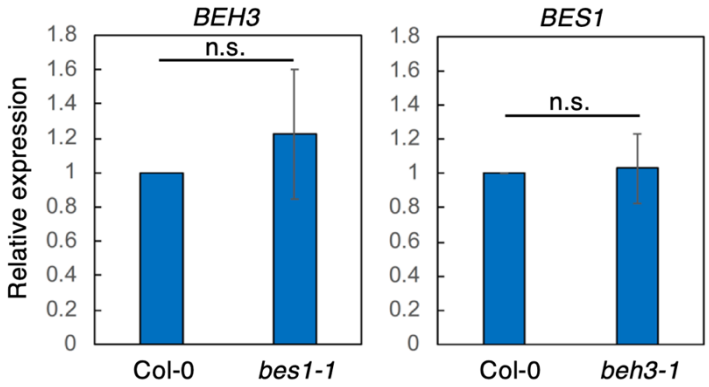

1004

1005 **Supplemental Figure 9. Expression levels of *BEH3* in *bes1-1* and *BES1* in**
1006 ***beh3-1* at 72 hours after VISUAL induction.** (Supports Figure 4)
1007 The data are indicated as relative fold change to Col-0 (**P*<0.05, ***P*<0.01;
1008 Student's t-test, *n* = 3, error bar = SD).

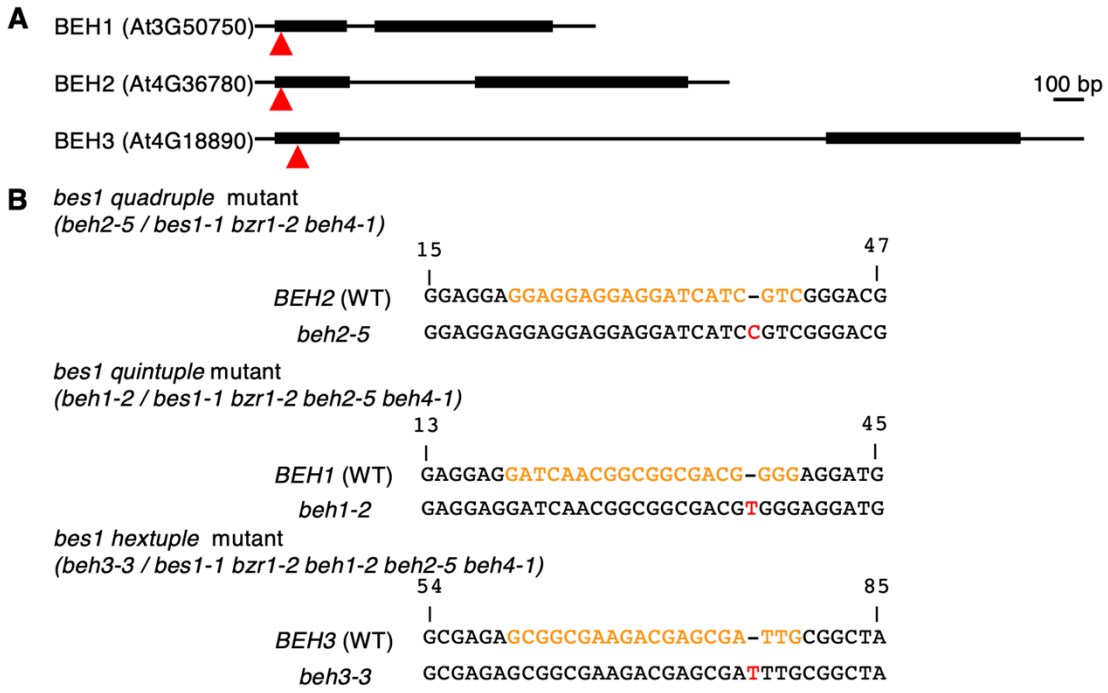

Supplemental Figure 10. Construction of genome-edited lines for BES/BZR homologs. (Supports Figure 6)

(A) Genomic structure of the encoding region of BEH1, BEH2, and BEH3. Red arrowheads indicate location of target site.

(B) The targeted sequence (orange) and a part of sequence in both wild-type line and mutant lines are shown. Each genome-edited line has a 1-bp insertion (red).

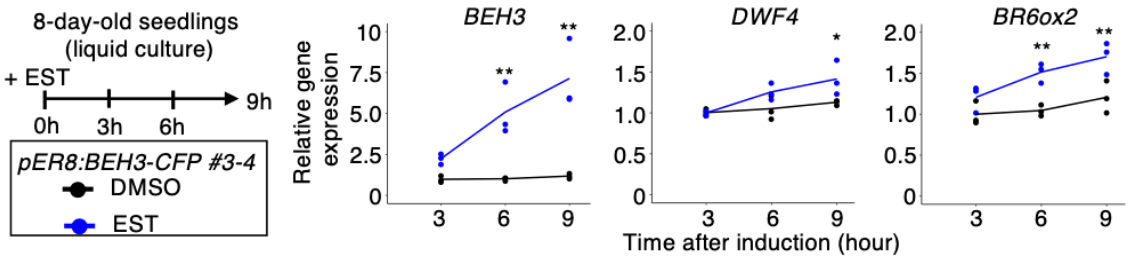

Supplemental Figure 11. Time-course expression analysis of BES/BZR target genes in the β-estradiol-inducible *BEH3* overexpression line. (Supports Figure 6)

Eight-day-old seedlings were treated with 10 μM β-estradiol to induce *BEH3* expression. Relative gene expression levels were calculated in comparison with the DMSO-treated sample at 3 h after induction (*$P < 0.05$, **$P < 0.01$; two-way ANOVA; $n = 3$). Values of statistical analysis listed in Supplemental Table 2.

1025 **Supplemental table 1. Results of two-way analysis of variance (ANOVA)**
1026 **for Figure 4E.**

IRX3 Method : Tukey

Factor	Level 1	Level 2	Average 1	Average 2	Difference	SE	Statistic	P value	* : P<0.05 ** : P<0.01
0h	*Col*	*bes1*	1.0000	1.0822	0.0822	12.0819	0.0068	1.0000	
	Col	*beh3*	1.0000	0.9405	0.0595	12.0819	0.0049	1.0000	
	Col	*bes1 beh3*	1.0000	0.9004	0.0996	12.0819	0.0082	1.0000	
	bes1	*beh3*	1.0822	0.9405	0.1416	12.0819	0.0117	1.0000	
	bes1	*bes1 beh3*	1.0822	0.9004	0.1818	12.0819	0.0150	1.0000	
	beh3	*bes1 beh3*	0.9405	0.9004	0.0402	12.0819	0.0033	1.0000	
24h	*Col*	*bes1*	6.7949	6.3790	0.4159	12.0819	0.0344	1.0000	
	Col	*beh3*	6.7949	8.8834	2.0886	12.0819	0.1729	0.9981	
	Col	*bes1 beh3*	6.7949	5.7313	1.0636	12.0819	0.0880	0.9997	
	bes1	*beh3*	6.3790	8.8834	2.5045	12.0819	0.2073	0.9968	
	bes1	*bes1 beh3*	6.3790	5.7313	0.6477	12.0819	0.0536	0.9999	
	beh3	*bes1 beh3*	8.8834	5.7313	3.1522	12.0819	0.2609	0.9936	
48h	*Col*	*bes1*	135.5941	13.7125	121.8816	12.0819	10.0880	P < 0.001	**
	Col	*beh3*	135.5941	173.1634	37.5692	12.0819	3.1096	0.0231	*
	Col	*bes1 beh3*	135.5941	132.2273	3.3668	12.0819	0.2787	0.9922	
	bes1	*beh3*	13.7125	173.1634	159.4509	12.0819	13.1975	P < 0.001	**
	bes1	*bes1 beh3*	13.7125	132.2273	118.5148	12.0819	9.8093	P < 0.001	**
	beh3	*bes1 beh3*	173.1634	132.2273	40.9360	12.0819	3.3882	0.0121	*
72h	*Col*	*bes1*	91.5413	50.4735	41.0677	12.0819	3.3991	0.0118	*
	Col	*beh3*	91.5413	74.2216	17.3197	12.0819	1.4335	0.4916	
	Col	*bes1 beh3*	91.5413	77.9913	13.5500	12.0819	1.1215	0.6801	
	bes1	*beh3*	50.4735	74.2216	23.7481	12.0819	1.9656	0.2287	
	bes1	*bes1 beh3*	50.4735	77.9913	27.5177	12.0819	2.2776	0.1316	
	beh3	*bes1 beh3*	74.2216	77.9913	3.7697	12.0819	0.3120	0.9892	

SEOR1 Method : Tukey

Factor	Level 1	Level 2	Average 1	Average 2	Difference	SE	Statistic	P value	* : P<0.05 ** : P<0.01
0h	*Col*	*bes1*	1.0000	1.3088	0.3088	10.1316	0.0305	1.0000	
	Col	*beh3*	1.0000	1.0357	0.0357	10.1316	0.0035	1.0000	
	Col	*bes1 beh3*	1.0000	0.8107	0.1893	10.1316	0.0187	1.0000	
	bes1	*beh3*	1.3088	1.0357	0.2730	10.1316	0.0269	1.0000	
	bes1	*bes1 beh3*	1.3088	0.8107	0.4981	10.1316	0.0492	1.0000	
	beh3	*bes1 beh3*	1.0357	0.8107	0.2251	10.1316	0.0222	1.0000	
24h	*Col*	*bes1*	9.3700	4.5883	4.7817	10.1316	0.4720	0.9645	
	Col	*beh3*	9.3700	14.3676	4.9975	10.1316	0.4933	0.9598	
	Col	*bes1 beh3*	9.3700	6.5691	2.8009	10.1316	0.2765	0.9924	
	bes1	*beh3*	4.5883	14.3676	9.7793	10.1316	0.9652	0.7701	
	bes1	*bes1 beh3*	4.5883	6.5691	1.9808	10.1316	0.1955	0.9973	
	beh3	*bes1 beh3*	14.3676	6.5691	7.7984	10.1316	0.7697	0.8673	
48h	*Col*	*bes1*	101.4912	56.0745	45.4167	10.1316	4.4827	P < 0.001	**
	Col	*beh3*	101.4912	135.2594	33.7682	10.1316	3.3330	0.0138	*
	Col	*bes1 beh3*	101.4912	94.9092	6.5820	10.1316	0.6497	0.9146	
	bes1	*beh3*	56.0745	135.2594	79.1849	10.1316	7.8156	P < 0.001	**
	bes1	*bes1 beh3*	56.0745	94.9092	38.8347	10.1316	3.8330	0.0042	**
	beh3	*bes1 beh3*	135.2594	94.9092	40.3502	10.1316	3.9826	0.0029	**
72h	*Col*	*bes1*	112.0916	97.0006	15.0910	10.1316	1.4895	0.4591	
	Col	*beh3*	112.0916	133.7105	21.6189	10.1316	2.1338	0.1712	
	Col	*bes1 beh3*	112.0916	120.2861	8.1945	10.1316	0.8088	0.8497	
	bes1	*beh3*	97.0006	133.7105	36.7099	10.1316	3.6233	0.0069	**
	bes1	*bes1 beh3*	97.0006	120.2861	23.2855	10.1316	2.2983	0.1266	
	beh3	*bes1 beh3*	133.7105	120.2861	13.4244	10.1316	1.3250	0.5566	

1027

1028

1029 **Supplemental table 2. Results of two-way analysis of variance (ANOVA)**

1030 **for Supplemental Figure 11.**

BEH3 Method : Tukey

Factor	Level 1	Level 2	Average 1	Average 2	Difference	SE	Statistic	P value	* : P<0.05 ** : P<0.01
3h	DMSO	Est	1.0000	2.2876	1.2876	0.9152	1.4068	0.1848	
6h	DMSO	Est	1.0340	5.1796	4.1456	0.9152	4.5295	P < 0.001	**
9h	DMSO	Est	1.2027	7.2724	6.0697	0.9152	6.6318	P < 0.001	**

BR6ox2 Method : Tukey

Factor	Level 1	Level 2	Average 1	Average 2	Difference	SE	Statistic	P value	* : P<0.05 ** : P<0.01
3h	DMSO	Est	1.0000	1.2068	0.2068	0.1267	1.6316	0.1287	
6h	DMSO	Est	1.0450	1.5146	0.4696	0.1267	3.7054	0.0030	**
9h	DMSO	Est	1.2062	1.7024	0.4961	0.1267	3.9144	0.0021	**

DWF4 Method : Tukey

Factor	Level 1	Level 2	Average 1	Average 2	Difference	SE	Statistic	P value	* : P<0.05 ** : P<0.01
3h	DMSO	Est	1.0000	0.9968	0.0032	0.0937	0.0340	0.9734	
6h	DMSO	Est	1.0486	1.2521	0.2035	0.0937	2.1705	0.0507	
9h	DMSO	Est	1.1264	1.4091	0.2827	0.0937	3.0160	0.0107	*

1031

1032 **Supplemental table 3. Sequences of sgRNA for CRISPR/Cas9 system.**

Oligo name	Sequence
BEH1-CRISPR-F	ATTGGATCAACGGCGGCGACGGGG
BEH1-CRISPR-R	AAACCCCCGTCGCCGCCGTTGATC
BEH2-CRISPR-F	ATTGGGAGGAGGAGGATCATCGTC
BEH2-CRISPR-R	AAACGACGATGATCCTCCTCCTCC
BEH3-CRISPR-F	ATTGGCGGCGAAGACGAGCGATTG
BEH3-CRISPR-R	AAACCAATCGCTCGTCTTCGCCGC

1033

1034 **Supplemental table 4. List of qRT-PCR primers.**

UBQ14	Left primer	TCCGGATCAGCAGAGGTT
	Right primer	TCTGGATGTTGTAGTCAGCAAGA
	Probe	#121
IRX3	Left primer	TGACATGAATGGTGACGTAGC
	Right primer	CATCAAATGCTCCTTATCACCTT
	Probe	#25
SEOR1	Left primer	AAGACACCAACGCCTCCA
	Right primer	CGATAGCATAGGAGACACTATCAAGA
	Probe	#136
ACT2	Left primer	CCGCTCTTTCTTTCCAAGC
	Right primer	CCGGTACCATTGTCACACAC
	Probe	#30
BEH3	Left primer	AATGTGGACTCCTGGACAA
	Right primer	CTGATCAACACCAGCAGGAA
	Probe	#108
DWF4	Left primer	TTCTCGTTATGACCAACCTAATCTC
	Right primer	AGGATGACGCTCCGTTGTT
	Probe	#145
BR6ox2	Left primer	CCCATGGAGATGGATGGA
	Right primer	CTTTCCAGGGCAAAGCCTA
	Probe	#10

1035